Rugged fitness landscapes minimize promiscuity in the evolution of transcriptional repressors

Anthony T. Meger[1,‡], Matthew A. Spence[2,‡], Mahakaran Sandhu[2], Colin J. Jackson[2,3,4,*], Srivatsan Raman[1,5,6,*]

[1]Department of Biochemistry, University of Wisconsin-Madison, Madison, Wisconsin 53706, United States

[2]Research School of Chemistry, Australian National University, Canberra, ACT 2601, Australia

[3]ARC Centre of Excellence for Innovations in Peptide & Protein Science, Research School of Chemistry, Australian National University, Canberra, ACT 2601, Australia

[4]ARC Centre of Excellence for Innovations in Synthetic Biology, Research School of Chemistry, Australian National University, Canberra, ACT 2601, Australia

[5]Department of Bacteriology, University of Wisconsin-Madison, Madison, Wisconsin 53706, United States

[6]Department of Chemical and Biological Engineering, University of Wisconsin-Madison, Madison, Wisconsin 53706, United States

[‡]These authors contributed equally to this work

Contact Information

*Corresponding authors: Colin Jackson (colin.jackson@anu.edu.au) and Srivatsan Raman (sraman4@wisc.edu)

ABSTRACT

How a protein's function influences the shape of its fitness landscape, smooth or rugged, is a fundamental question in evolutionary biochemistry. Smooth landscapes arise when incremental mutational steps lead to a progressive change in function, as commonly seen in enzymes and binding proteins. On the other hand, rugged landscapes are poorly understood because of the inherent unpredictability of how sequence changes affect function. Here, we experimentally characterize the entire sequence phylogeny, comprising 1158 extant and ancestral sequences, of the DNA-binding domain (DBD) of the LacI/GalR transcriptional repressor family. Our analysis revealed an extremely rugged landscape with rapid switching of specificity even between adjacent nodes. Further, the ruggedness arises due to the necessity of the repressor to simultaneously evolve specificity for asymmetric operators and disfavors potentially adverse regulatory crosstalk. Our study provides fundamental insight into evolutionary, molecular, and biophysical rules of genetic regulation through the lens of fitness landscapes.

KEYWORDS: ancestral sequence reconstruction (ASR); protein evolution; deep mutational scanning (DMS); epistasis; sequence space; fitness landscape

INTRODUCTION

A central question in molecular evolution is how proteins acquire novel functions, such as new binding specificities, via mutation and selection. The sequence-fitness landscape is a valuable construct that has allowed us to understand and visualize the complex relationship between evolutionary sequence changes and protein function.[1–5] The topology of a fitness landscape largely reflects the nature of the evolutionary process: “smooth” landscapes, with small numbers of discrete but connected peaks across which new activities can gradually evolve via additive and predictable mutational steps, are relatively well understood, with many enzymes and binding proteins as examples.[2,6–10] The molecular basis for the smoothness of these transitions can be partly explained by the modulation of the conformational dynamics of proteins, in which mutations can gradually shift the conformational equilibrium towards conformations better suited to the new activity.[11–13] In contrast, our understanding and characterization of “rugged” fitness landscapes, in which mutations tend to have unpredictable epistatic effects that result in fitness landscapes consisting of multiple peaks separated by many non-functional sequences (“valleys”), is less well developed.[14–16] One intriguing hypothesis is that the sequence-fitness landscapes of certain proteins are inherently defined by the function and fold.[17] This partially deterministic view has important implications for evolution of new activities (such as drug[17,18] or vaccine resistance[19]) and protein engineering. [20,21]

To understand and characterize the role of rugged fitness landscapes in molecular evolution, we need to comprehensively map sequence-function relationships over large and diverse sequence spaces that span the full evolutionary history of protein families. While directed evolution and deep mutational scanning (DMS) experiments have provided profound insight into molecular evolution at the level of single mutational steps, they seldom explore the large evolutionary timescales and the full diversity of sequence space within protein families.[4,7] In contrast, ancestral sequence reconstruction (ASR) can sample large spans of sequence space through the computational

68 reconstruction of ancestral species from a phylogenetic tree and a sequence evolution model.[22,23]
69 However, ASR studies generally characterize a relatively small number of divergent ancestral
70 sequences, which makes it difficult to deconvolute adaptive and neutral mutations and understand
71 the stepwise additive and context-specific (epistatic) effects of mutations.[24]
72
73 In contrast to enzymes, which have been shown to often evolve across relatively smooth fitness
74 landscapes in which promiscuous activities can be gradually optimized to become the primary
75 function,[11–13] transcription factors likely display a more rugged fitness landscape as they are
76 generally defined by high DNA specificity, and incremental mutations leading to promiscuity could
77 be evolutionarily disfavored. The lac repressor (LacI), which belongs to the LacI/GalR family
78 (LGF) of prokaryotic gene regulators,[25] is a well-studied model for DNA recognition and allostery.[26]
79 Proteins of the LGF show remarkable diversity in their amino acid sequences and their DNA
80 recognition. While much is known about the operator specificity of *Escherichia coli* LacI
81 (EcLacI),[27–31] our understanding of the sequence-fitness landscape of DNA-binding specificity in
82 the wider LGF, the historical evolutionary trajectory of operator recognition and the molecular
83 mechanisms that underpin the evolution of DNA-specificity in proteins remains incomplete. The
84 LGF is thus a compelling system to study ruggedness in sequence-fitness landscapes and how
85 the combination of structure and function dictate the evolutionary dynamics and selective
86 pressures exerted on these regulators.
87
88 In this study, we experimentally characterize a complete phylogenetic tree (1158 extant and
89 ancestral sequences) of the LGF and perform DMS on extant EcLacI to reveal the sequence-
90 fitness landscape of DNA specificity for the *E. coli* Lac operator. We find the landscape to be
91 extremely rugged due to high levels of epistasis, with most sequences having no affinity for the
92 *E. coli* lac operator sequence. However, the screen unearthed dozens of functional repressors
93 from distinct phylogenetic clades, with as many as 32/60 amino acid substitutions in the DNA

binding domain (DBD) compared to the EcLacI DBD. Analysis of the local evolutionary landscape within clades shows gain/loss of function between adjacent nodes, indicating rapid switches of specificity, which may be beneficial for developing orthogonal genetic regulation. The ruggedness of this fitness landscape may therefore be a characteristic feature of regulators and an essential functional requirement of high specificity and orthogonality. The molecular basis for this observation is revealed through *in vitro* binding assays and simulations, which show that ruggedness of the LGF fitness landscape arises in part due to the necessity for regulators to simultaneously evolve specificity for either DNA half-site in asymmetric operators and explains why this fold and operator structure has been evolutionarily selected for genetic regulation. This study provides new fundamental insight into nature's design of genetic regulation, evolutionary rules of protein-DNA recognition, the biophysical mechanism of transcription factor allostery, and how structure and function combine to determine the sequence-fitness landscapes of proteins.

RESULTS

Synthesis and characterization of a complete phylogeny of LGF DNA-binding domains. The *E. coli* lac operator sequence has emerged over a ~3-billion-year evolutionary history. To generate a set of DBDs that spans the full evolutionarily accessible sequence space of the LGF, we performed phylogenetic inference to reconstruct 577 ancestral sequences from a dataset of 581 extant EcLacI homologs (**Fig. 1a**). Consistent with previous phylogenetic studies,[32] our analysis reconstructs the family as three major lineages. When rooted at the phylogenetic midpoint, these include the LacI-clade as the most ancestral, a single common ancestor giving rise to descendent clades comprising the catabolite control protein (CcpA/RegA), ribose, maltose, sucrose, galactose, arbutin/salicin, purine and cytosine regulators (RbsR, MalR, SacR/ScrR, GalR/GalS, AscG, PurR and CytR, respectively), and an uncharacterized lineage of LacI-like proteins (**Fig. 1a**). On average, the mean posterior probability of each ancestral DBD was 93%, indicating strong statistical support across the full dataset (**Supplementary Fig. 1a**). Likewise,

120 phylogenetic branch supports were consistently high across the topology (**Supplementary Fig.**
121 **1b**), and the approximately unbiased test failed to reject the topology we present in Fig. 1 among
122 9 other tree-search replicates (P-value=0.682)[33] (**Supplementary Fig. 2**).
123
124 One limitation of ASR is that, while it is possible to generate hundreds of ancestral sequences
125 computationally, only a handful (<10) of evolutionarily distant nodes are typically characterized
126 experimentally. Thus, the incremental functional adaptations associated with the full evolutionary
127 trajectory can remain obscured by neutral variation. Here, we synthesized the DBDs of all 577
128 reconstructed ancestors, as well as all 581 extant sequences used in our phylogeny, generating
129 a dataset of 1158 diverse DBDs that fully covers the phylogenetic tree constructed in this work
130 (**Fig. 1a**). We used chip-based oligonucleotides to synthesize the DBD sequences and cloned
131 them into a plasmid library to encode chimeric variants consisting of DBDs fused to the ligand-
132 binding domain (LBD) of EcLacI, which is induced by allolactose/IPTG (**Fig. 1b**). We constructed
133 chimeras with an invariant LBD for several reasons: (i) by studying the ancestral DBD in the
134 context of the EcLacI LBD, we can be confident that the regulatory mode of the chimeras will
135 match that of the extant EcLacI and will repress in the absence of an allosteric effector;[34] (ii) since
136 the inducer of the EcLacI LBD is known, we can study the allosteric communication between LBD
137 and DBD in the chimeras; (iii) we can ensure that the experimental conditions we used were
138 conducive to repression, giving accurate insight on exclusively DNA specificity in the DBD. Deep
139 sequencing the plasmid library confirmed 100% coverage of the DBD library with minimal skew
140 i.e., all 1158 DBDs were present (**Supplementary Fig. 3**).
141
142

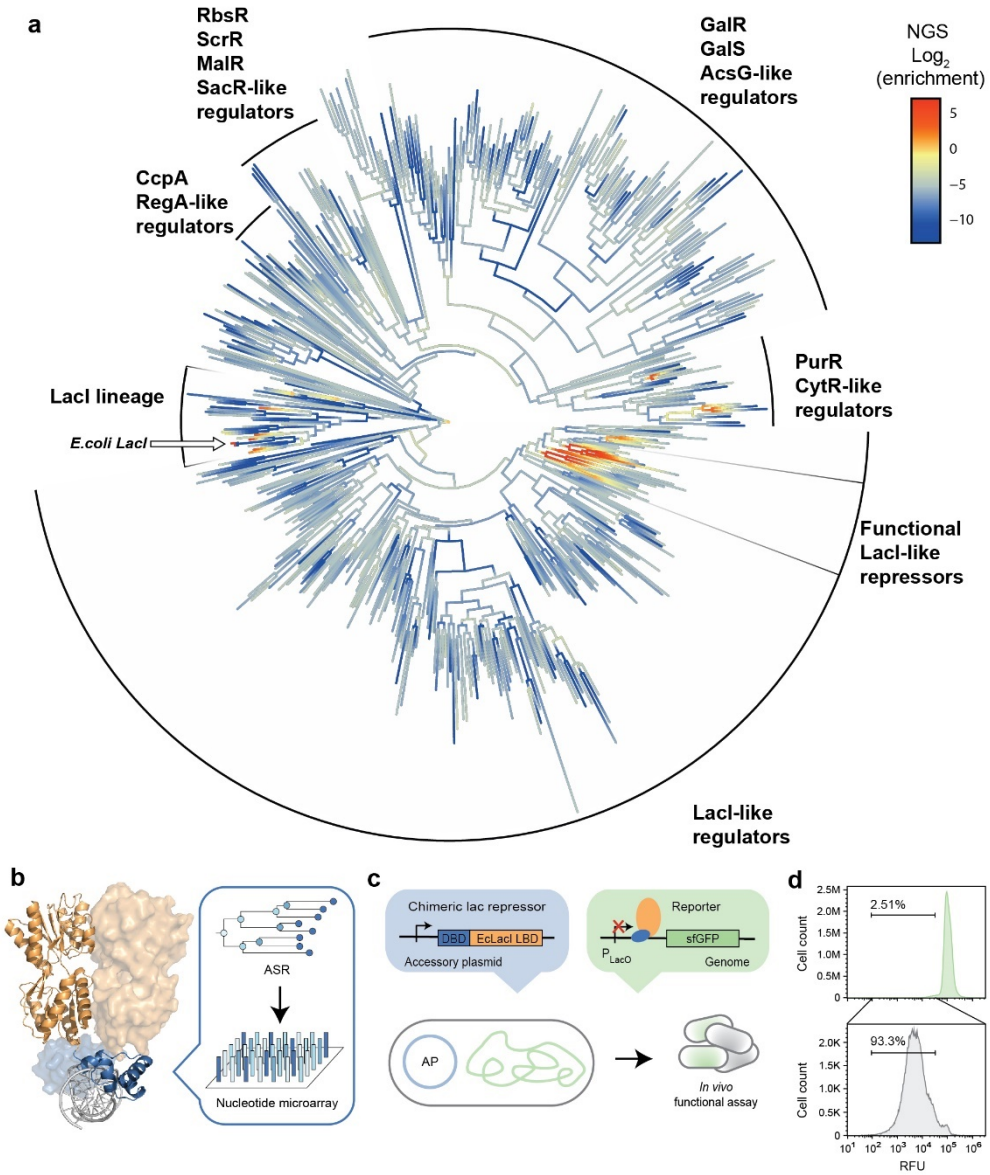

Fig. 1. Evolution of LacO recognition. (**a**), Phylogenetic inference of the LacI/GalR family of prokaryotic transcription factors. 577 sequences were ancestrally reconstructed using from a dataset of 581 extant LacI homologs (**Supplementary Fig. 1,** see "methods"). Color gradient shows average repression scores from replicate (*n*=2) high-throughput screens (**Supplementary Fig. 4**). (**b**), Structure (PDB ID: 1EFA) of dimeric extant *E. coli* lac repressor bound to LacO (left). LBD (orange), DBD (blue), and LacO (gray) are shown in cartoon representation. Each extant and ancestral DBD was generated using multiplex micro-array DNA synthesis (right). (**c**), *In vivo* characterization of repressor function. DBDs were fused to the *E. coli* LacI LBD and constitutively expressed on an accessory plasmid. A reporter construct consisting of the gene encoding sfGFP under transcriptional control of LacO was integrated into the genome of E. coli to assay repressor function. (**d**), Flow cytometry of the pre-selected phylogenetic DBD library (top) and after two sequential sorts to isolate repression competent DBDs (bottom). The indicated gate was used for selection by FACS (**Supplementary Fig. 4**). RFU, relative fluorescence units.

157 To characterize the affinity of the DBDs within the phylogeny to the *E. coli* lac operator and their
158 allosteric activation by IPTG, we used a cell-based pooled screening strategy (**Fig. 1c**). We
159 inserted a single-copy GFP cassette under the control of the lac operator (LacO) into the *E. coli*
160 genome. Variants that can bind to LacO with sufficient affinity repress GFP expression, while
161 those that cannot produce high GFP expression. Using fluorescence-activated cell sorting
162 (FACS), repression-competent variants are enriched by sorting low GFP cells. Only a small
163 fraction (2.5-2.6%) of low-fluorescence cells were observed via flow cytometry, indicating that
164 relatively few extant and ancestral DBDs in this library repress LacO (**Fig. 1d**). The subset of
165 repression competent variants was enriched to 92.7-93.3% of the total population after two rounds
166 of sorting (**Supplementary Fig. 4**). The pre- and post-sorted libraries were sequenced to estimate
167 the enrichment ratios. A higher enrichment ratio implies greater GFP repression and is a proxy
168 for protein-DNA affinity. The enrichment ratios were highly correlated (R^2=0.99) between
169 independent replicates (**Supplementary Fig. 5**). We found 15 ancestral and 7 extant DBDs that
170 can repress GFP from the 1158-member library. These 22 enriched DBDs comprise 1.9% of the
171 1158-member library, consistent with the fraction of the low-fluorescence population observed via
172 flow cytometry.
173
174 **The sequence-fitness landscape of the DNA binding domains is rugged.** A fundamental
175 question in molecular evolution is whether the emergence of new functions is mediated by the
176 gradual partitioning of functions (smooth) or by discrete switches (rugged). On a smooth fitness
177 landscape, we would expect a single lineage to exhibit gradual changes in activity and maintain
178 significant promiscuity. For example, the binding specificities of proteins within the periplasmic
179 amino acid binding protein family (same fold as the LBD of the LGF family) were shown to
180 gradually alter over time along evolutionary lineages through the selection of promiscuous
181 functions.[24,35] In contrast, a rugged fitness landscape involving discrete specificity switches, would
182 result in different functions being sparsely dispersed across the phylogeny. Our results reveal an

183 extraordinarily rugged fitness landscape for the DBDs, in which functional repressors are
184 dispersed within multiple lineages across the phylogenetic tree (**Fig. 1a, Fig. 2a-c**). Indeed, *LacO*
185 repression appears to have emerged in three evolutionarily distinct lineages; the EcLacI clade,
186 PurR/CytR clade and a third clade that we dub the functional LacI-like regulators. Notably, these
187 clades are evolutionarily distinct and share an ancestor only at the LCA of the full LGF, which
188 diverged ~3Gya.
189
190 We next traced the evolution of function within the clade in which *LacO* repression was observed,
191 showing that recognition of LacO is sporadic within each group. For instance, in the EcLacI clade,
192 out of the 28 ancestral sequences, only seven were repression competent. Additionally, we
193 identify 32 instances where LacO recognition is either gained or lost between adjacent nodes
194 (**Fig. 2a-c**). Thus, while evolutionary selection and optimization of ancestral function exist to some
195 extent, we observe that rapid gain or loss of that same function is more dominant across the LGF
196 phylogeny. In summary, the DBDs of the LGF family appear to be evolving across a rugged fitness
197 landscape, leading to rapid gain/loss of function transitions.

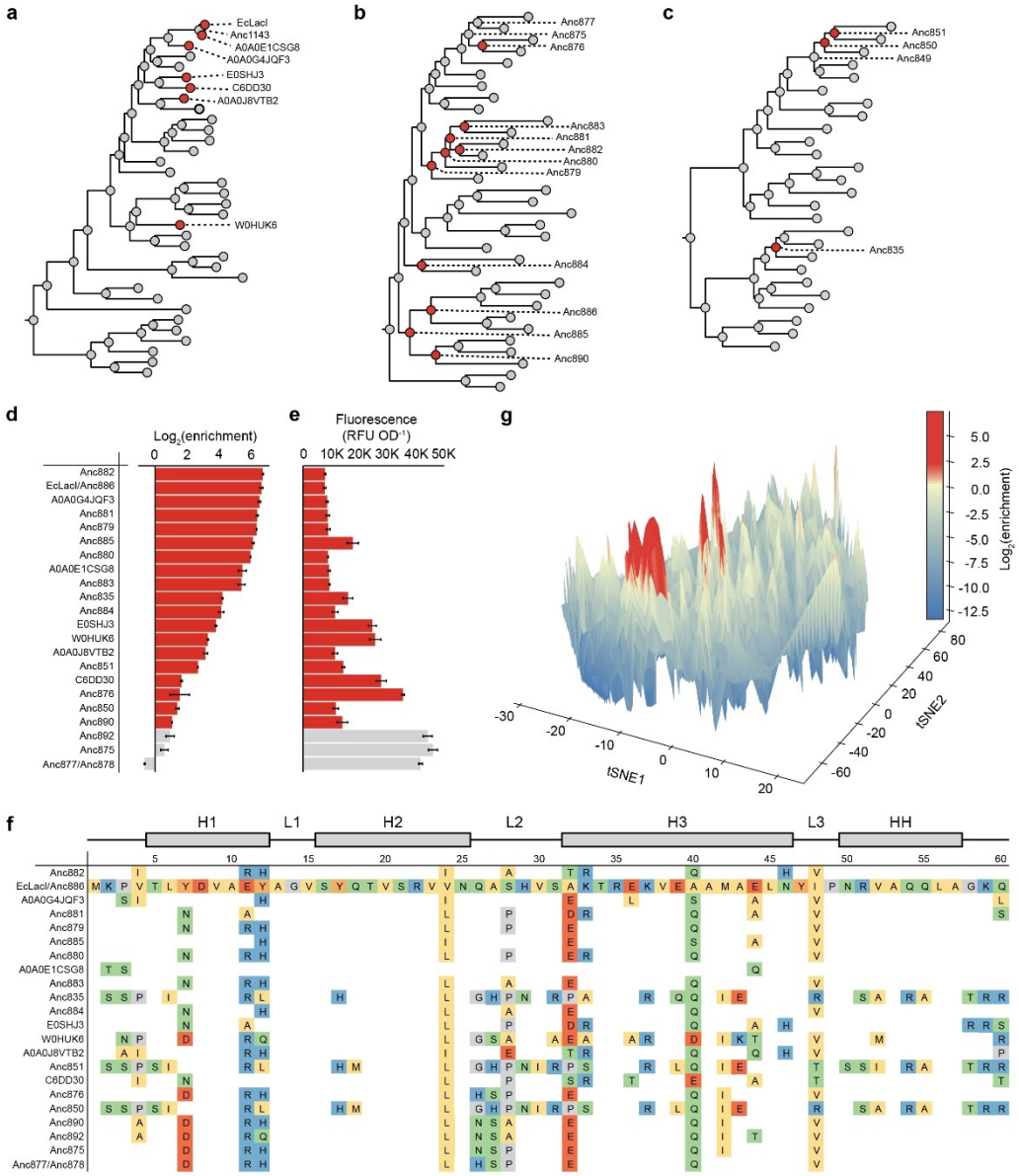

198

199 **Fig. 2. Sequence-fitness landscape and phylogenetic mapping of LacO recognition.** (**a-c**),
200 Lineages containing functional repressors of LacO. Ancestrally reconstructed sequences are
201 numbered by tree node and extant sequences are indicated with UniProt IDs. Red nodes indicate
202 clonally validated functional repressors of LacO within the LacI lineage (**a**), functional LacI-like
203 regulators (**b**), and PurR/CytR-like regulators (**c**), and gray nodes indicate non-functional
204 repressors. (**d**)**,** Extant and ancestral DBD variants with the greatest enrichment from our high-
205 throughput screens. Enrichment values were determined by comparing NGS distributions of the
206 pre- and post-sorted populations. Error bars denote the standard deviation of replicate (n=2)
207 sorting and NGS experiments. (**e**), Clonally assayed mean fluorescence values (n≥2) normalized
208 to OD_{600}. (**f**), Primary sequences of characterized ancestral and extant DBDs and overall
209 structural topology of the DBD (top). (**g**), Sequence-fitness landscape of repressor function.
210 Enrichment values were mapped onto the t-SNE landscape of the UniRep represented
211 phylogenetic DBD sequences (see “methods”) to assay ruggedness. RFU, relative fluorescence
212 units. OD, optical density.

213 To understand how and why sequence changes altered LacO recognition, we investigated the
214 enrichment of different sequences, which showed a strong correlation between the enrichment
215 ratio and the ability of a variant to repress (**Fig. 2d-f, Supplementary Fig. 6)**. Clonal screening
216 revealed a near-binary functional switch in repression competency separating enriched and
217 depleted variants (**Fig. 2d,e**). Of the 1158-member variant library, 7 extant and 13 ancestral
218 sequences were clonally validated as repression competent. Analysis of the sequence
219 conservation patterns revealed among the four helices of the DBD, H2 and HH are most
220 conserved as these are essential for LacO recognition and allosteric activation, respectively (**Fig.
221 2f; Supplementary Fig. 7**).[36] Indeed, within the recognition helix (H2) residues Tyr17, Gln18 and
222 Arg22, which directly interact with the lac operator and control DNA specificity[37], are rarely
223 mutated in the functionally repressive DBDs. The only exceptions include Y17H and Q18M, which
224 have both been demonstrated to maintain lac operator binding in the genetic background of
225 *Ec*LacI.[38,39] Notably, ancestors 835, 850, and 851 have multiple substitutions in the HH; these
226 variants repress GFP but are not allosterically activated by 1 mM IPTG (**Supplementary Fig. 8**),
227 consistent with the role of HH in allosteric signaling.[36]
228
229 To obtain a global view of the sequence-function landscape, we encoded the DBD sequences as
230 high dimensional vectors with unified representation (UniRep), a deep learning model that allows
231 sequences with similar structural, functional, and evolutionary properties to be clustered together
232 in space (**Fig. 2g**).[40] This highlights the extreme ruggedness of the sequence-function landscape,
233 with three regions that correspond to the LacI lineage, functional LacI-like regulators, and
234 PurR/CytR-like regulators, containing most of the functional peaks. The rugged surface and
235 isolated functional peaks suggest that there is little promiscuous binding across the family, that
236 there is extreme epistasis with a small and finite number of functional sequences, and that there
237 is low robustness or tolerance to mutations. In summary, our broad analysis of LacO repressor
238 function across the 1158 sequences of this phylogenetic tree suggests that (a) LacO recognition

239 is an easily accessible evolutionary state (appeared independently multiple times) and (b) it
240 simultaneously exists within narrowly confined solution spaces (the fitness peaks that do exist are
241 very small and surrounded by inactive sequences).
242
243 **Diverse substitutions shape local ruggedness among related DBDs.** To better understand
244 how the sequence space surrounding the functional repressors affects function, we identified
245 specific mutations that affect function. This is challenging in genetically diverse datasets because
246 neutral genetic drift and epistasis can both mask and confound sequence-function relationships.
247 In this dataset, the context-dependence of three amino acid positions, 18, 22, and 26, illustrate
248 how epistasis creates ruggedness (**Fig. 2a-c**). First: Gln18 in the non-functional ancestor Anc849
249 is mutated to Met18 (previously shown to increase affinity (2.5-fold) to LacO in EcLacI[39]) in
250 Anc850 (alongside Glu39Leu), resulting in gain of function, followed by the introduction of
251 Arg48Thr, Asn50Ser, and Ala52Ile in Anc851, which retains function even though these mutations
252 are highly represented in non-functional variants (**Fig. 2c; Supplementary Fig. 9**). Thus, the
253 deleterious effects of Arg48Thr, Asn50Ser, and Ala52Ile are mitigated by the presence of
254 Gln18Met.[41] Second: Arg22 is essential for LacO binding as it forms a critical base-specific
255 hydrogen bond (**Supplementary Fig. 7b**);[42]while it is found in every functional variant in the
256 screen (**Fig. 2f**), 1018 non-functional variants also contain Arg22. Arg22His is among the
257 substitutions found in Anc1143, which is the closest non-functional ancestor of EcLacI (**Fig. 2a**).
258 Third: Asn26 in the non-functional ancestor Anc875 is mutated to His26 in Anc876 and introduces
259 function *de novo*. However, when Asn26His is introduced alongside the Ile42Met in Anc877, there
260 is no gain of function (**Fig. 2b**). In summary, we find subtle mutational perturbations have large
261 effects on function, indicating a metastable state, and that epistasis contributes to the ruggedness
262 of the landscape.
263

264 **Historical contingency and genetic drift shape evolution.** While evolutionary trajectories of
265 proteins are constrained by biological function, stochastically sampled permissive substitutions
266 also shape the sequence landscape and contribute to historical contingency i.e., the dependence
267 of evolutionary trajectories on historical mutations.[43–45] From ASR alone, it is difficult to parse
268 whether mutations are functionally essential, permissive, or neutral because ancestral and extant
269 sequences are often separated by many substitutions. Therefore, to investigate the role of each
270 DBD position, we used deep mutational scanning (DMS), to systematically assay all single-amino
271 acid substitutions in EcLacI. By combining ASR with a DMS screen of EcLacI, we sought to
272 disentangle conserved residues that have been fixed by adaptive evolution from those that arose
273 through neutral drift.
274
275 To functionally characterize all single amino acid substitutions of the *Ec*LacI DBD (1121 variants
276 in total), we used the same technologies (oligonucleotide chip synthesis, one-pot library cloning,
277 FACS, and deep sequencing) as described previously for our high-throughput phylogenetic
278 screen (**Supplementary Fig. 10**). We sorted the low fluorescence population to enrich the
279 repression-competent variants. The number of repression-competent DMS variants (25% of the
280 population) was 10-fold higher than from the phylogenetic library (2.5%) (**Supplementary Fig.
281 11a**). These were enriched to ~95% of the population after two rounds of sorting (**Supplementary
282 Fig. 11b,c**). Sequencing of pre- and post-sorted libraries yielded enrichment ratios, normalized to
283 native EcLacI, that were highly correlated (R^2=0.93) between independent replicates
284 (**Supplementary Figs. 12**)[31].

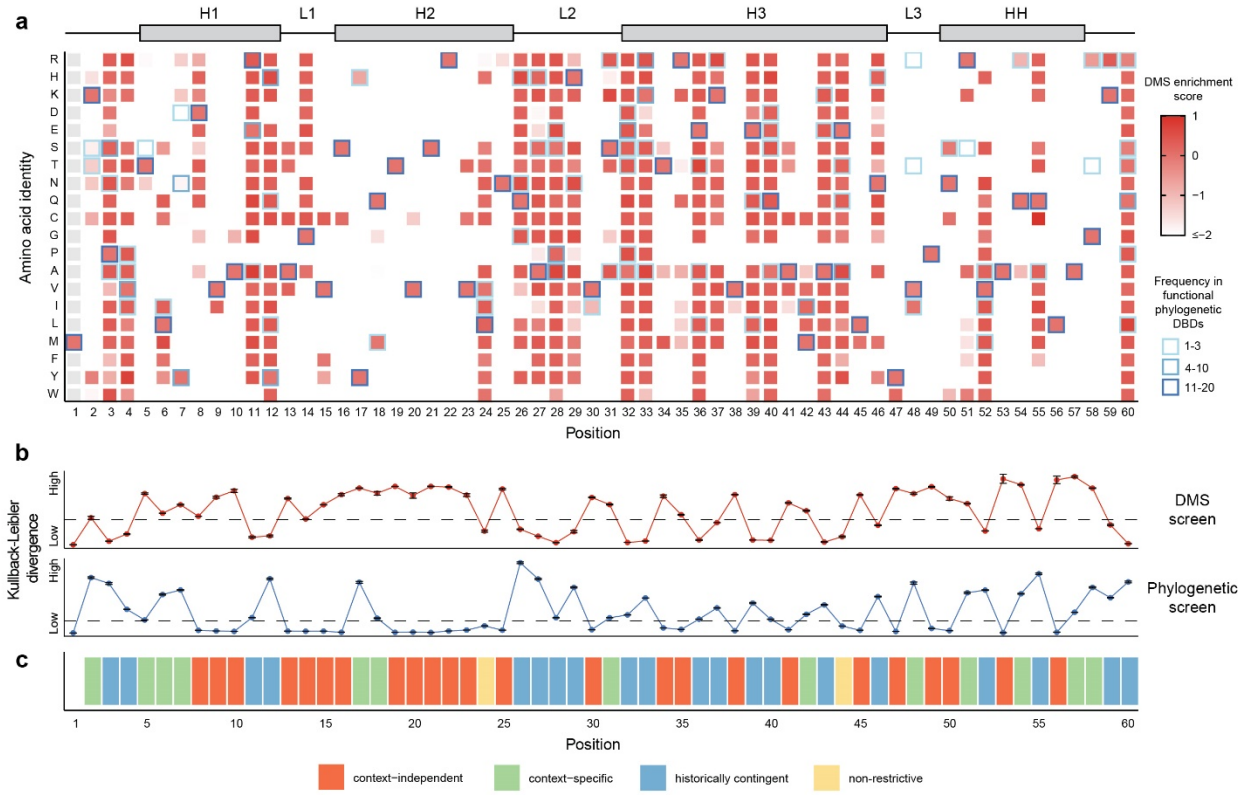

Fig. 3. DMS to assign evolutionary roles to each position of the DBD. (**a**), Heat map showing the normalized enrichment scores (red gradient) of each EcLacI substitution after selection of repression competent DBDs. Secondary structure topology of the DBD (top) and substitution frequency (blue gradient) among functional extant and ancestral DBDs are shown. (**b**), Kullback-Liebler divergence (KLD) describes how much the amino acid probability distribution changes at each position in response to functional selection in both the DMS and phylogenetic screens. For the DMS screen, positions with high KLD are functionally restrictive, whereas low KLD positions are more tolerant to substitutions. (**c**), Assigned evolutionary roles to each DBD position based on KLD analysis of the DMS and phylogenetic screens. Context-independent positions (low phylogenetic KLD and high DMS KLD) contribute to stability and general HTH fold. Context-specific positions (high phylogenetic and DMS KLD) modulate LacO recognition. Historically contingent positions (high phylogenetic KLD and low DMS KLD) are not functionally constrained in the genetic background of *E. coli* LacI, despite sequence convergence among functional phylogenetic variants. Non-restrictive positions (low phylogenetic and DMS KLD) are generally tolerant to substitutions.

For this DMS experiment, each DBD position has a probability distribution of the 20 canonical amino acids pre- and post-selection. We used Kullback-Lieber divergence (KLD[46]; a statistical method for comparing two probability distributions) to discern which residues are functionally restrictive (high score) and non-restrictive (low score). This showed that the restrictive and non-

306 restrictive positions are non-uniformly distributed across the DBD, with H2 and HH largely
307 intolerant to substitutions (**Fig. 3a, b**), consistent with the sequencing results from the phylogeny
308 (**Fig. 2**), while the C-terminus, loop 1, loop 2 and most of H3 are robust to mutation.
309
310 While DMS provided key insights into the functional role of each residue, it lacks an evolutionary
311 perspective. For instance, using DMS alone we cannot distinguish between residues essential for
312 LacO recognition ("context-specific") and those required for stability and general fold ("context-
313 independent"). By combining DMS with our extensive phylogenetic screen, it is possible to define
314 an evolutionary role for each residue (**Fig. 3b**). There are four possible combinations of DMS
315 (high/low) and phylogenetic (high/low) KLD scores, each representing a unique evolutionary role
316 of a residue (**Fig. 3c**). Context-independent functionally restrictive residues, such as those that
317 are structurally essential, have high DMS KLD scores (functionally restrictive) and low
318 phylogenetic KLD scores - because positions that are conserved across all phylogenetic variants
319 cannot undergo a shift in probability distribution upon selection and thus have low KLD scores
320 despite potentially being functionally relevant (**Fig. 4a,b**). These context-independent residues
321 are heavily concentrated within the core of the HTH fold and across the dimerization interface of
322 the HH, and include essential LacO-binding residues, such as Arg22 (**Fig. 4a,b**). Context-
323 dependent functionally restrictive positions have high KLD scores for both DMS and phylogenetic
324 screens. These residues are critical for LacO recognition, either making direct contact with the
325 operator DNA in both the major and minor grooves, helping to orient the DBD for LacO binding,
326 or interacting with the LBD for allosteric communication. Context-dependent residues include
327 Tyr7, Tyr17 and Gln18 and Met42 – all of which contact LacO or are associated with an epistatic
328 change-of-function, such as in Anc877 (**Fig. 4c,d**). Historically contingent positions have low DMS
329 and high phylogenetic KLD scores i.e., while mutationally robust in terms of EcLacI function, they
330 are restricted in phylogenetic analysis owning to their deterministic role in evolution (**Fig. 4e,f**).
331 Many of these residues are located adjacent to context-dependent functionally restrictive

positions, consistent with a role in modulating their effect, such as Asn26 (historically contingent) and Met42 (context-specific) (**Fig 4f**). Functionally non-restrictive positions have low KLD scores for both DMS and phylogenetic screens. Only two solvent-exposed residues, Val24 and Glu44, fall within this category. Altogether, this analysis demonstrates that the evolutionary role of all residues within the DBD of EcLacI can be revealed through a statistical analysis of DMS and ASR data.

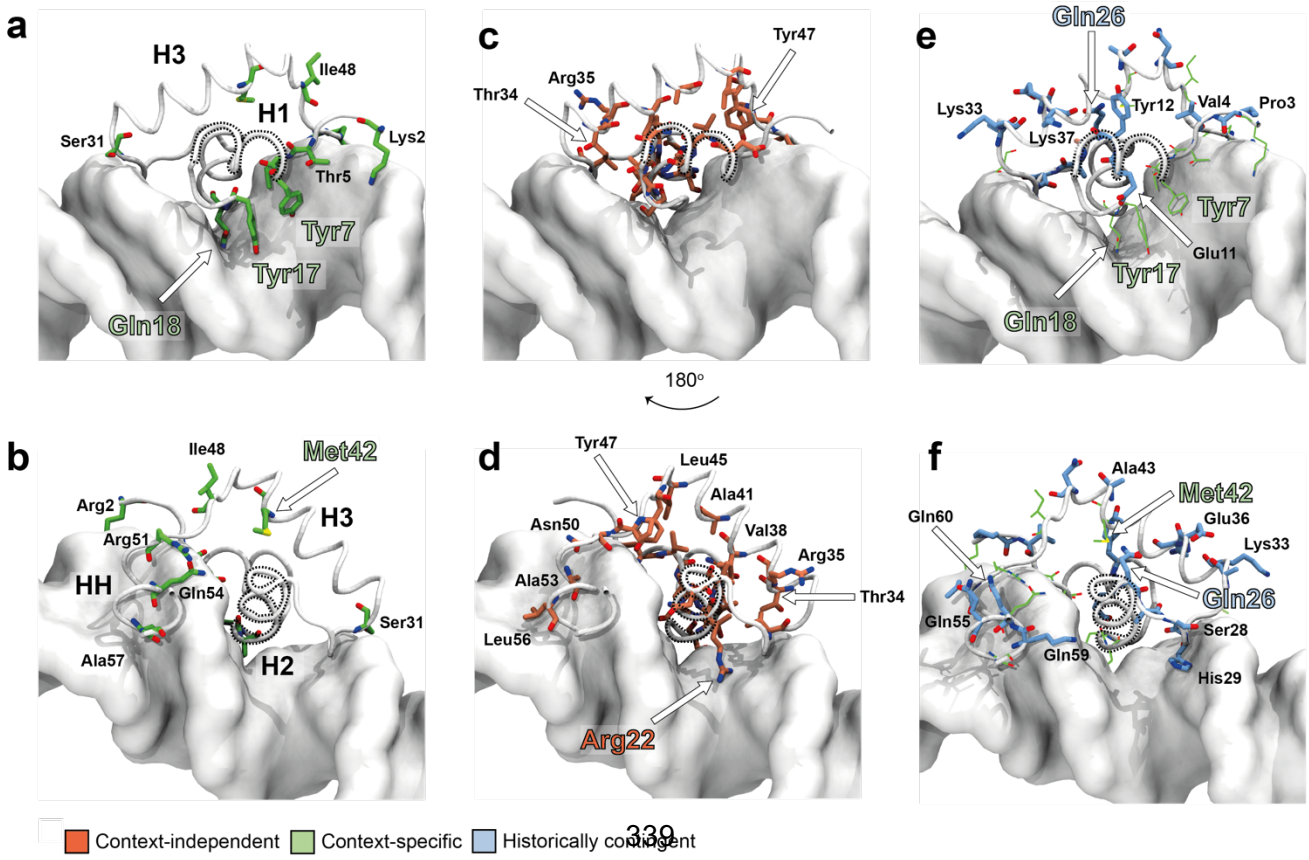

Fig. 4. Structural role of DBD mutations. (a) Context-specific mutations in the LacO major groove, where Tyr7, Tyr17 and Gln18 make essential contacts with the DNA. (b) context-specific mutations in the minor groove. Context-specific mutations are dominated by locations that contact the DNA, particularly in the major groove. (c) Context-independent mutations in the major groove. Context-independent mutations cluster around the core packing of the DBD. (d) Context-independent mutations in the minor groove. Context-independent mutations also include those essential for DNA-recognition, such as Arg22. (e) Historically contingent mutations in the major groove. Context specific mutations are represented as lines (green), historically contingent are represented as sticks (cyan). (f) Historically contingent mutations in the minor groove. Historically contingent mutations cluster around the context specific mutations that they set the background for. For example, Met42 and Gln26 (epistatically linked) are oriented towards one another on H3 and H1, respectively.

353

354 **Operator asymmetry contributes to the rugged fitness landscape.** Despite asymmetric DNA
355 operator sequences having lower affinity for DBDs than symmetrical sequences,[47] they are
356 overwhelmingly dominant throughout evolution and must therefore confer some selective benefit.
357 To investigate this, we performed *in vitro* DNA-binding assays using surface plasmon resonance
358 (SPR; **Fig. 5**). We find that all functional variants tested (Anc880, Anc881 and Anc882) bind the
359 symmetrical $LacO_{sym}$ with K_d constants greater than an order of magnitude lower than their
360 asymmetric operator counterparts (LacO and $LacO_1$), confirming that operator asymmetry
361 significantly reduces a repressor's DNA-binding capacity in ancestral, as well as extant DBDs
362 (**Fig. 5a-c**; **Supplementary Fig. 13**).

363

364 To investigate the molecular basis for binding of asymmetrical operator sequences, we performed
365 all-atom molecular dynamics (MD) simulations on models of Anc880 and 882, as well as EcLacI,
366 complexed with LacO (**Fig. 5**). Each system was simulated with 10 independent 60 ns replicates
367 (600 ns total sampling time) (**Supplementary Fig. 14**). Previous studies have identified motions
368 related to DNA-binding specificity in *Ec*LacI occur over ns – μs timescales, consistent with the
369 timescale of our simulations.[48,49] We observe asymmetry in the protein-DNA interactions between
370 the two monomers that constitute the functional dimer (**Fig. 5d,e**). Although both monomers
371 interact with the DNA via the same residues, the relative contributions these residues make to the
372 overall binding energy and their DNA contacts are distinct. In Anc882, which is the variant with
373 the greatest LacO affinity, we identified Tyr7, Tyr17, Gln18 and Arg22 as being essential for DNA
374 recognition and binding. However, the conformations of each of these residues differ between
375 monomers to accommodate the respective operator half-sites and principal component analysis
376 (PCA) reveals that backbone motions differ between either monomer (**Fig. 5d-f**). Identical
377 analyses of apo-Anc882 trajectories found that in the absence of DNA, backbone motions are
378 nearly indistinguishable between monomers (**Supplementary Fig.14**). This analysis is consistent

379 with NMR structures of the EcLacI DBD complexed with the natural $LacO_1$ operator[50], and
380 alternate DNA binding modes have been alluded to by analyses of LGF repressors and EcLacI
381 mutants.[51] Thus, asymmetrical operator sequences impose a complex selective pressure: the
382 DBDs must be able to undergo a conformational change to bind two distinct half-sequences with
383 physiologically relevant affinity. Being subject to multiple selection pressures associated with
384 either half-site to maintain complete operator binding is consistent with the extreme ruggedness
385 we observe (**Fig. 2**).

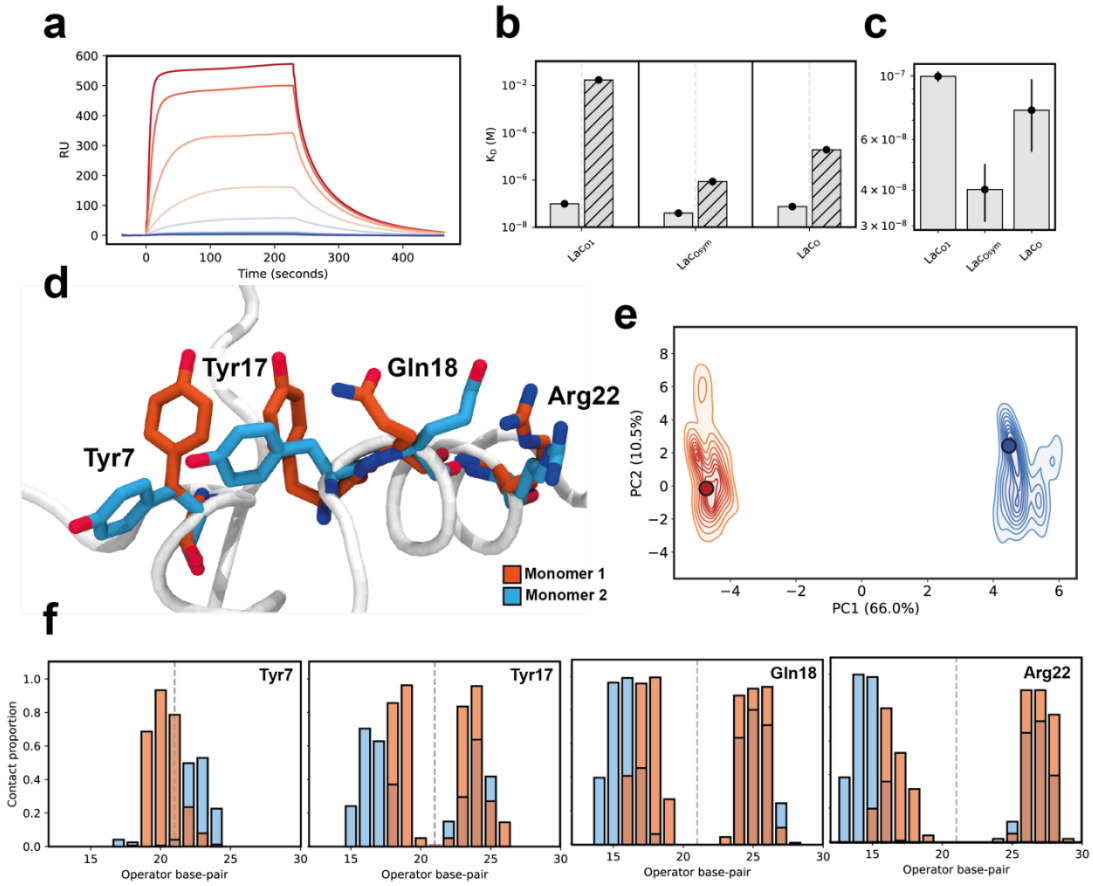

386 **Fig. 5**
387 **Transcriptional regulator asymmetry and fitness landscape ruggedness.** (a) Multi-cycle
388 kinetics SPR sensogram for Anc882 LacO binding. (b) Anc882 K_d values, determined by SPR for
389 $LacO_1$, $LacO_{sym}$ and LacO DNA binding when repressed (solid) and induced with 10 mM IPTG
390 (hashed). (c) Magnified view of repressed K_d values. (d) Conformational snapshots of the most
391 sampled conformations for monomers 1 (red) and 2 (cyan). Dominant conformations of Tyr7,
392 Tyr17, Gln18 and Arg22 are shown from principal component analysis (PCA; panel e). (e) PCA
393 of Anc882, showing monomers A (red) and B (blue). Conformational snapshots presented in (d)
394 are shown as circles. (f) Distribution of key protein-DNA contacts in Anc882 and LacO. DNA
395 residues (X-axis) have been aligned for visualization.

396 The demand on the DBD to simultaneously evolve high affinity for two distinct half-site DNA
397 sequences using a single binding site (as well as allosteric regulation with the LBD) means that
398 the fitness landscape we observe across this phylogeny can be viewed as a composite of two or
399 more fitness landscapes. To test this, we performed *in silico* evolutionary simulations on small
400 model systems using theoretical elementary landscapes as a model (**Fig. 6**)[52–54]. Elementary
401 landscapes derive from a robust and well-established graph-theoretic approach to combinatorial
402 landscape optimization problems[54]; specifically, they are the orthogonal eigenvectors of the
403 graph-Laplacian of a sequence space graph. For our purposes, they provide a theoretically
404 rigorous way of testing hypotheses that pertain to the ruggedness of a fitness landscape. Using
405 a linear combination of elementary landscapes, each representing a different hypothetical fitness
406 function, we find that the combination of two fitness landscapes can indeed be more rugged than
407 either constitutive fitness landscape is alone, akin to constructive/deconstructive wave
408 interference (**Fig. 6**). This demonstrates that ruggedness can emerge from the composition of
409 otherwise smooth fitness landscapes and predicts that proteins with a single function, such as
410 enzymes or solute binding proteins, may evolve over smoother fitness landscapes than proteins
411 such as LGF repressors, where multiple and complex fitness constraints are imposed
412 simultaneously.
413

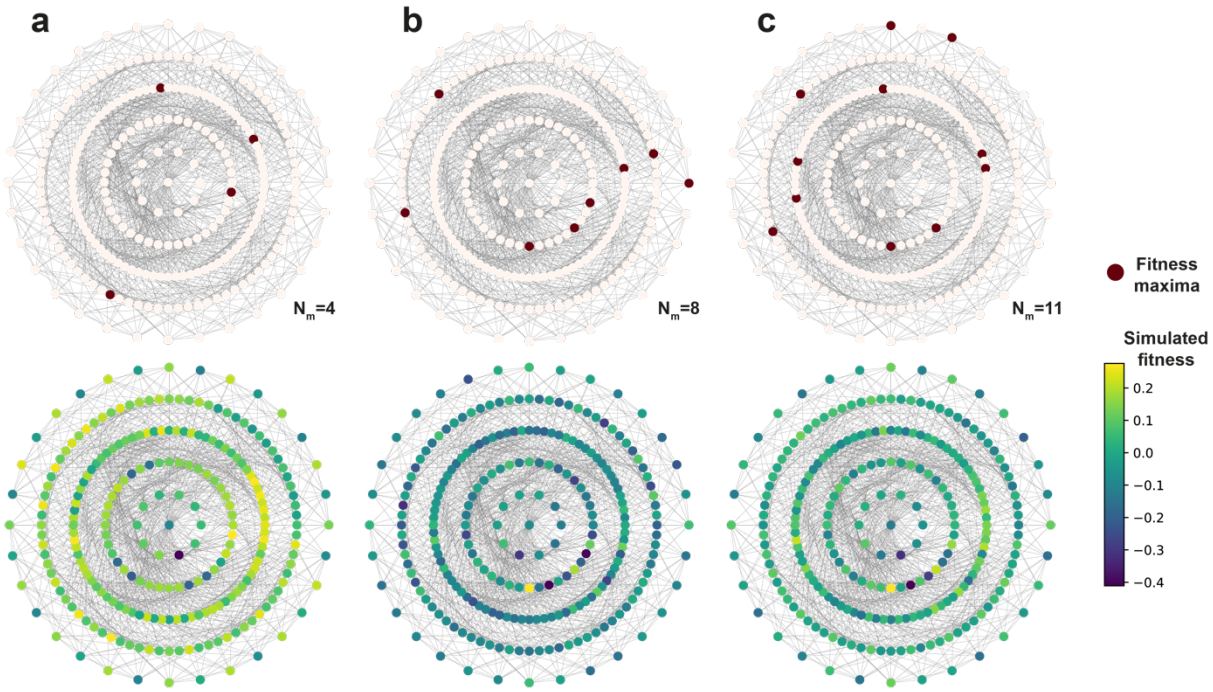

Fig 6. Elementary landscape model simulations. 2nd and 3rd elementary landscapes in panels (a), (b) respectively. Each vertex represents a unique genotype, colored fitness maxima (top) and quantitative simulated fitness (bottom). Edges connect genotypes accessible by a single mutation. (a) and (b) have 4 and 8 fitness maxima (N_m), respectively (where N_m is the number of fitness peaks where all neighboring genotypes have a lower fitness). (c) A linear combination of 2nd and 3rd elementary landscapes. The composite landscape is characterized by 11 fitness maxima, more than either constituent landscape, and is more rugged.

DISCUSSION

These results show that the fitness landscape for operator binding by DBDs of the LGF is extremely rugged i.e., the viable fitness space for LacO recognition and repression is narrow and highly localized. Interestingly, this ruggedness has long been alluded to by mutational studies, but never comprehensively observed or studied prior to our work.[5] In contrast, most of the protein families studied by ASR to date demonstrate protein evolution over smooth fitness landscapes where gradual changes in function can be observed.[24,35,45,55–58] Even those characterized by extensive epistasis have well-defined mutational trajectories from semi- or non-functional intermediate sequences to functional ones[44,59]. The profound difference in evolutionary dynamics between these studies and the LGF may reflect fundamentally different biological and physical

433 constraints. While any complex molecular trait can be described as a combination of arbitrarily
434 smooth fitness functions (i.e. folding, substrate-recognition, electrostatic preorganization,
435 immunogenicity, among many catalytic and structural parameters[60]) DNA recognition among LGF
436 regulators is particularly rugged due to the compounding of two DNA-binding landscapes that
437 likely have complexity in isolation; if either half-site requires the correct folding, dynamical
438 ensemble, electrostatic and shape complementarity (among likely many other traits), a protein
439 sequence that binds both half-sites must compound the molecular requirements for both of the
440 half-sites.
441
442 One notable aspect of the rugged DBD landscape is the evolutionary metastability of repression:
443 descendants of a repression competent ancestor are seldom functional with the same operator
444 sequence and mutations have extreme epistatic relationships. This indicates that both selection
445 pressure for LacO specificity has been variable and that LacO specificity has emerged
446 independently numerous times throughout evolutionary history, each time in different sequence
447 contexts. Like the notion of an epistatic ratchet, where a phenotype becomes completely
448 inaccessible within a specific background[43,61], the metastability we observe occurs through non-
449 specific mutations that counteract or reciprocate the fitness effects of previously fixed mutations
450 in backgrounds that are on the edge of a binary phenotype, making a few genetic changes
451 sufficient to rewire specificity. Using a combination of ASR and DMS, we have comprehensively
452 mapped historical contingency within the DBD showing that permissive sites, which are essential
453 in an evolutionary context and underlie the epistasis and metastability, can be identified.
454
455 The rugged landscape, the asymmetry of the DBD:DNA complex and the evolutionary
456 metastability of the repressor function are all interesting observations, but how do they relate to
457 the physiological role of these proteins? Since effective genetic regulation is paramount to
458 organismal fitness, precise and binary interactions are essential. To impart a selective advantage,

459 regulators must be highly specific for their cognate operator sequences. Unlike promiscuous
460 enzymatic activity, promiscuous DNA-binding causes metabolic cross-regulation and severe
461 disruption of cellular function.[62,63] Thus, we hypothesize that this ruggedness fitness landscape is
462 an intrinsic aspect of fitness for the LGF: asymmetric operator half-sites have evolved as a
463 mechanism to minimize metabolic crosstalk between regulators and create an evolutionary
464 dynamic in which activity is essentially binary. Over a rugged fitness landscape, as we observe,
465 DNA-binding specificity is metastable, with rapid gain/loss of function, essentially eliminating the
466 risk of non-specific DNA-binding and metabolic cross-regulation between diverging regulators.
467 This suggests that inherently epistatic protein folds, such as that of the DBD, have likely been
468 evolutionarily selected for regulatory purposes. Indeed, previous ASR studies have shown that
469 epistasis is a hallmark of several classes of eukaryotic transcription factors,[59,64–67] and recent
470 results have highlighted the importance of molecular unpredictability in transcription factor
471 divergence.[68] Interestingly, similar observations of rapid *de novo* promoter emergence have also
472 recently been made, indicating that the evolutionary dynamics we observe in regulatory proteins
473 may also be present in their DNA binding partners.[69]
474
475 Altogether, our analysis of the sequence-function landscape of the LGF DBDs has led to several
476 valuable insights. Most importantly, we prove a molecular level explanation for the high fidelity
477 that has long been observed in gene regulation by proteins of the LGF family, showing that it is
478 an intrinsic property of the rugged fitness landscape that is itself a function of the biophysical
479 properties of DBD structure and asymmetry of DNA operator sequences. Future work could
480 investigate whether rugged fitness landscapes, and functional partitioning through asymmetry,
481 are common when the physiological function of the protein family makes promiscuous activity
482 deleterious, as for these transcriptional regulators.
483
484

485 **METHODS**

486 **Phylogenetic inference**

487 To collate an expansive dataset of the full LGF, EcLacI, RbsR, MalR, SacR/ScrR, GalR, GalS,
488 AscG, PurR, CytR, and CcpA were each individually queried against the NCBI non-redundant
489 protein database using pBLAST. ~250 sequences were retrieved from each individual BLAST
490 search, using an e-value significance threshold of 1.0E-10. Redundancy in this dataset was
491 removed to 90% sequence identity using CD-HIT[70] and incomplete sequences, or sequences with
492 poorly conserved (<1% of sequences) indels were manually removed. Sequences were aligned
493 using the ESPRESSO protocol of T-COFFEE. [71] This alignment was manually refined to remove
494 poorly conserved sequences or insertions and benchmarked against available LGF X-ray crystal
495 structures. Phylogenetic inference was performed in IQ-TREE.[72] The ML model, LG+R9,[73,74] was
496 fitted using ModelFinder (as implemented in IQ-TREE).[74] Tree-search was performed using
497 default parameters and branch supports were computed as ultra-fast bootstrap approximations.[75]
498 Tree search was repeated for 10 independent replicates, which were tested for statistical
499 equivalency by the approximately unbiased (AU) test conducted to 10000 replicates.[33] An
500 additional inference was performed using the same protocol, however, only including the N-
501 terminal 60 columns of the LGF dataset to determine how much evolutionary signal the DBD
502 provides to the full-length sequences (Supplementary Fig 2). Ancestral sequences were
503 reconstructed on the single topology presented in Fig. 1 using CodeML from the PAML software
504 package.[76] The sequence evolution model for ASR was manually set to LG+G4[73] and indel events
505 were processed in the ancestral sequences according to the principle of parsimony.

506

507 **Construction of GFP reporter strain**

508 The *E. coli* strain DH10β was modified by lambda Red recombineering to insert a superfolder
509 GFP gene driven by the pLlacO[77] promoter and a kanamycin resistance cassette at the LacI locus
510 to generate the GFP "reporter" cell line. The temperature sensitive plasmid pKD46 (Genbank

511 AY048746) was used for arabinose-inducible expression of Red recombinase.[78] Linear double-
512 stranded donor DNA was amplified off a pSC101 plasmid using overhang primers to add 50bp
513 homology arms directed to the 5' end of the LacI gene. A frozen glycerol stock of DH10β
514 transformed with the pKD46 plasmid was struck out on LB carbenicillin (100µg/mL) and incubated
515 at 30°C overnight. A colony was selected and inoculated into 5mL LB carbenicillin and grown for
516 16h in a shaking incubator at 30°C. Cells were diluted 50X into 25mL of LB carbenicillin and grown
517 to an OD of 0.1. Red recombinase was induced with 100mM L-arabinose and cells were grown
518 to an OD of 0.6. The cells were harvested and prepared for electroporation. 25µL of cells were
519 transformed with 500ng of donor DNA. Cells were recovered for 2h in SOC media in a shaking
520 incubator at 37°C and plated on LB kanamycin (30 µg/mL). The transformants were incubated at
521 37°C overnight to cure the cells of the temperature sensitive pKD46 plasmid. A visibly fluorescent
522 colony was selected and inoculated into 5mL LB kanamycin to be grown for 16h in a shaking
523 incubator at 37°C. The genome modification was confirmed via sequencing and a glycerol stock
524 was stored at -80°C.
525
526 **General library DNA assembly**
527 Plasmids were constructed using standard molecular biology techniques of PCR and Golden Gate
528 assembly with Kapa HiFi DNA Polymerase (KAPA Biosystems), restriction enzymes (NEB), T4
529 DNA Ligase (NEB), and Antarctic Phosphatase (NEB).
530
531 Oligonucleotides encoding residues 2-60 of all LGF DBDs (1158 variants in total) or all single
532 amino acid substitutions of the *E. coli* LacI DBD (1121 variants in total) were synthesized as
533 single-stranded oligonucleotide pools (Agilent Technologies). Extant DBDs exceeding 60aa long
534 were truncated from the N-terminus to 60 residues in length to comply with DNA synthesis
535 restrictions. Oligonucleotides were converted to double-stranded DNA using 15 cycles of PCR
536 amplification and purified on a spin column (EZNA Cycle Pure kit from Omega BioTek). A pSC101

537 backbone containing extant *E. coli* LacI gene under control of the strong pLtetO promoter and a
538 spectinomycin resistance gene was amplified using a primer pair encoding BsaI cut sites that
539 matched the DBD insertion location of both oligonucleotide libraries. The amplified backbone was
540 treated with Dpn1 for 2h at 37°C and purified using a spin column. The backbone was treated
541 with BsaI-HF v2 for 2h at 37°C, Antarctic phosphatase for 1h at 37°C, and subsequently purified
542 using a spin column. A Golden Gate assembly reaction (30 cycles of 37°C for 5min and 16°C for
543 5min) was performed using 0.042 pmol pSC101 backbone and 0.21 pmol amplified DBD library
544 in a 1:5 molar ratio. The assembled product was dialyzed on a semi-permeable membrane
545 (Millipore) for 1h at 25°C against dH_2O. A 25µL aliquot of electrocompetent DH10β *E. coli* cells
546 were transformed with 2µL of the dialyzed product using electroporation. Cells were recovered
547 for 1h in SOC media in a shaking incubator at 37°C and dilutions were plated on LB Spectinomycin
548 (50 µg/mL) to calculate transformation efficiency (>10^6 CFU/mL). Remaining recovered cells were
549 diluted 5x, incubated for 6h, and then diluted 50X for overnight growth in a shaking at 37°C for
550 16h. Library plasmids were extracted using a DNA miniprep kit and 1µL (~100ng) was used to
551 transform 25µL of electrocompetent reporter cells following the transformation protocol described
552 above. Glycerol stocks of the reporter cells transformed by the preselected phylogenetic and DMS
553 plasmid libraries were stored at -80°C.
554
555 **Fluorescence-activated cell sorting**
556 Thawed glycerol stocks of reporter cells containing the LGF DBD or DMS libraries were used to
557 inoculate (50µL each) 5mL of LB kanamycin (30µg/mL) / spectinomycin (50µg/mL) in duplicate.
558 Cells were grown in a shaking incubator at 37°C for 16h and subsequently diluted 50X in PBS
559 (137mM NaCl, 2.7mM KCl, 10mM Na2HPO4, 1.8mM KH2PO4) for sorting. Sorting was performed
560 with a Sony MA900 cell sorter. Cells were excited with a 488nm laser and GFP fluorescence was
561 monitored through a 525/50 filter. A sorting gate was drawn to isolate the low-fluorescence
562 populations of the LGF DBD (2.5-2.6% of total population, 250,000 cells collected) and DMS

563 (25.4-25.6% of total population, 500,000 cells collected) libraries. Cells were sorted into 1mL of
564 LB, and the total volume was adjusted to 5mL after sorting. Cells recovered for 1h at 37°C in a
565 shaking incubator before antibiotics were added (kanamycin and spectinomycin), and incubation
566 was continued for another 15h. Glycerol stocks were made and stored at -80°C. Plasmids were
567 harvested using a DNA miniprep kit and 1μL (~100ng) was used to transform 25μL of fresh
568 electrocompetent reporter cells. The procedure described above was repeated for a second round
569 of low-fluorescence sorting using the same sorting gates to further enrich for repression
570 competent variants.
571
572 **Next-generation sequencing**
573 We used deep sequencing to evaluate presorted and sorted LGF and DMS populations. The DBD
574 was amplified in two stages with Kapa HiFi DNA Polymerase (KAPA Biosystems) for tailed
575 amplicon sequencing. The first PCR reaction was performed with overhang primers that anneal
576 to 5' and 3' constant regions surrounding the DBD. The overhangs add a variable N region (to
577 enhance nucleotide diversity), and a portion of the universal Illumina adapter. The first reaction
578 was performed using 14 cycles with 1ng of extracted plasmid DNA (DMS or LGF library, presorted
579 or sorted) as template. The product was purified on a spin column (EZNA Cycle Pure kit from
580 Omega BioTek). A second PCR reaction was used to add the index (for pooled sequencing) and
581 the Illumina 'stem'. This amplification was performed using 10 cycles with 10ng of the purified
582 product from the first reaction as template. The amplicons were purified and used for deep
583 sequencing. Samples were sequenced on an Illumina MiSeq System, using a MiSeq Reagent Kit
584 v2 (2x250 cycles) following the manufacturer's documentation.
585
586 Paired-end Illumina sequencing reads were merged with PEAR (Paired-end read merger).[79]
587 Phred scores (Q scores) were used for quality filtering. Reads with an expected number of errors
588 exceeding 1 were removed and total read counts for each DBD variant were computed

589 (**Supplementary Figs. 3,10**). Raw read counts were highly correlated ($R^2 \geq 0.97$) for all replicate
590 samples. Enrichment for each variant was computed using

591 $$Enrichment = \frac{f_{sorted}}{f_{presorted}}, \qquad (eq. 1)$$

592 where $f_{presorted}$ and f_{sorted} are relative read count frequencies before and after enrichment of
593 repression competent variants, respectively. Higher enrichment indicates tighter repression of
594 GFP and higher affinity to LacO. For the DMS library, enrichment scores (Escore) were computed
595 by normalizing enrichment to WT and applying a log2 transformation. Thus, the WT DMS Escore
596 is set to 0, Escore > 0 indicates improved function, and Escore < 0 indicates reduced function.
597
598 Kullback-Liebler divergence of a specific position is given by the following:

599 $$KLD = \sum_{a} f_{sorted,a} \log_2 \frac{f_{sorted,a}}{f_{presorted,a}}, \qquad (eq. 2)$$

600 where the sum is over all 20 canonical amino acid identities, and $f_{sorted,a}$ and $f_{presorted,a}$ are the
601 relative frequencies of an amino acid a in the repressed sorted or presorted distributions,
602 respectively. If the relative frequency of an amino acid at a position is zero, then the value was
603 excluded from the summation.
604
605 **Microplate fluorescence assay for clonal characterization**
606 The presorted and repressed sorted LGF DBD libraries were struck out on LB kanamycin
607 (30μg/mL) / spectinomycin (50μg/mL) plates. Colonies were selected and inoculated into 150μL
608 LB kanamycin/spectinomycin in a 96-well plate. Cells were incubated at 37°C in a microplate
609 shaker for 8h. The cultures were diluted 50X in fresh media in a 96-well plate with varying
610 concentrations of IPTG (0, 0.1, 0.5, 1, 5, 25, 100 and 1000μM). Diluted cultures were incubated
611 at 37°C in a microplate shaker for 14h. GFP fluorescence and OD_{600} were measured in a BioTek
612 Synergy HTX Multi-Mode 96-well plate reader. Fluorescence was normalized to OD to account

613 for differences in cell density. Assayed colonies were sequenced to identify the DBD variant. The
614 mean and standard deviation of normalized fluorescence for replicates (n ≥ 2) for each
615 concentration of IPTG were used to fit these dose-response curves to the Hill–Langmuir equation:

616 $$fluoresence = b + \frac{(F_{max} - b)[x]^n}{EC_{50}^n + [x]^n}, \qquad (eq.3)$$

617 where b is the basal fluorescence (measure of LacO affinity in the absence of inducer), F_{max} is
618 the maximum fluorescence signal achieved at 1mM IPTG, EC_{50} is the half maximal effective
619 concentration, x is the concentration of IPTG, and n is the Hill coefficient.

620

621 **Protein expression and purification**

622 Anc880, 881 and 882 were synthesized and cloned into the NdeI/XhoI multiple cloning site of
623 pET-28a(+) with a C-terminal 6x histidine tag. All three ancestral proteins were recombinantly
624 expressed in BL21(DE3) lab strain *E. coli* at 25 °C for 16 hours in Luria-Bertani (LB) media. Protein
625 expression was induced with 10 mM IPTG once media OD_{600} reached approximately 1.5 AU. Cells
626 were pelleted by centrifugation at 5,000 RPM for 15 minutes and were lysed by sonication once
627 resuspended in buffer A [20 mM PBS, 150 mM NaCl, 20 mM imidazole (pH 7.4)] containing the
628 recommended amount of *Serratia marscecens* Turbonuclease (Sigma-Aldrich). The lysate was
629 pelleted by centrifugation at 12,000 RPM, 4 °C for 1 hour before being filtered (0.22 μM) and
630 loaded onto a prepacked 5 mL HisTrap FF immobilized metal ion affinity chromatography column
631 (GE lifescience) equilibrated in buffer A. The loaded column was washed for 5 column volumes
632 in buffer A and 3 column volumes in 94% buffer A/ 6% buffer B [20 mM PBS, 150 mM NaCl, 250
633 mM imidazole (pH 7.4)], before being eluted with 100% buffer B on an AKTA Start FPLC
634 instrument (GE lifescience). IMAC purified protein was then filtered (0.22 μM) and purified by size
635 exclusion chromatography (SEC) on a prepacked HiLoad superdex 200 16/60 SEC column (GE
636 lifescience) equilibrated in SEC buffer [20 mM PBS, 150 mM NaCl (pH 7.4)] and run on an AKTA
637 FPLC system (GE lifescience).

638

639 **Surface Plasmon resonance**

640 Proteins purified to homogeneity by IMAC and SEC were buffer exchanged into SPR running
641 buffer [10 mM HEPES, 300 mM NaCl, 3 mM EDTA, 0.05% (v/v) tween-20 (pH 7.4)] and diluted
642 into a $\log_2$ dilution series from 250 nM - 3.91 nM for repressed binding samples and 10 μM – 78.1
643 nM for samples induced with 70 μM IPTG. $_{\text{Double}}$-stranded DNA oligonucleotides for LacO,(
644 TGTGTGGAATTGTTATCCGCTCACAATTTCACACA) $LacO_1$
645 (TGTGTGGAATTGTGAGCGGATAACAATTTCACACA), $LacO_{sym}$
646 (TGTGTGGAATTGTGAGCGCTCACAATTTCACACA), and random DNA
647 (AGGTCAAAAAGCCAGTGGTTATTTTAAGATGTCGC) were synthesized and 5'-biotinylated
648 (IDT). All SPR experiments were performed on a Biacore 8K instrument (GE lifescience). An SA
649 streptavidin Biacore chip (GE lifescience) was activated with 1 M NaCl and 20 mM NaOH before
650 four channels were charged with approximately 400 RU of each respective DNA ligand. Binding
651 affinity was determined through multi-cycle kinetic analysis at the 7 serial $\log_2$ protein dilutions,
652 and one buffer only blank. All protein analytes were run at 50 μL/min for a ligand contact time of
653 120 seconds. After each analyte cycle, the ligand was regenerated with 3 M NaCl run at 20 μL/min
654 for a contact time of 60 seconds. The K_d of DNA binding was determined from a multi-cycle model
655 fitted to the reference subtracted sensorgrams in the Biacore 8K evaluation software.

656

657 **Molecular dynamics simulations**

658 Models for Anc880 and Anc882 were generated from X-ray crystallography coordinates of EcLacI
659 bound to $LacO_{sym}$ (PDB: 1EFA)[80] using FoldX[81]. The $LacO_{sym}$ DNA ligand in 1EFA was mutated
660 to the LacO sequence that was experimentally tested using X3DNA. [82] To avoid DNA terminal
661 fraying, 5' and 3' termini were extended with sequences GGAAT and TCC respectively in X3DNA
662 for all models (Full DNA sequence: GGAATTGTTATCCGCTCACAATTCC). Simulations were

663 performed in the GROMACS MD engine using the Amber ff14SB[83] force field with PARMBSC1[84]
664 nucleic acid parameter set. MD integration used a timestep of 2 fs. Columb interactions were
665 modelled using particle mesh Ewald (PME) with a cut-off radius of 1.0 nm. Leonard-Jones
666 interactions used a cut-off scheme with a radius of 1.0 nm. Hydrogen bonds were constrained
667 using the LINCS algorithm. [85] For each system, 10 independent replicates of equilibration (from
668 the NVT ensemble onwards) and production MD were performed. Each protein-DNA complex
669 was put in a rhombic dodecahedral box extending at least 1.0 nm from the closest atom to the
670 box boundary in all directions. Simulation boxes were filled with TIP3P water molecules, and the
671 charge was neutralized with sodium and chloride ions. To replicate physiological conditions, each
672 box was additionally filled with 150 mM NaCl. All systems were energy minimized by steepest
673 descent with a step size of 0.01 nm until the greatest force was less than 1000 KJ/mol/nm. The
674 systems were equilibrated to 300 K in the NVT ensemble with harmonic restraints on all heavy
675 atoms for 100 ps using a velocity rescale thermostat and brought to 1 Bar pressure in the NPT
676 ensemble for 100 ps using a Berendsen barostat. Following temperature and pressure
677 equilibration, unrestrained production MD was performed for 100 ns in the NPT ensemble using
678 a velocity rescale thermostat and a Parrinello-Rahman barostat with references of 300 K and 1
679 Bar, respectively. Following periodic boundary corrections, all trajectories were analyzed in
680 MDTraj and every 10th frame was sampled. All production MD was performed on the Australian
681 National Computing Infrastructure GADI supercomputer.
682
683 **Elementary landscape simulations**
684 Elementary landscapes were calculated via eigendecomposition of the graph adjacency matrix
685 corresponding to a combinatorial sequence space over an alphabet of 3 amino acids and 5
686 number of positions. Elementary landscapes were indexed by order (e.g. first-order, second-order
687 and so on), and composition of landscapes performed combinatorically between 1st and 2nd
688 order, 1st and 3rd order, and 1st and 3rd order landscapes. The composition operation was

defined as a simple linear combination of landscapes (in analogy to superposition of waves in physics). All graph construction and matrix operations were performed in NumPy and Networkx. The number of local maxima were calculated using custom functions. Graph plotting was performed in Networkx using custom functions.

ACKNOWLEDGEMENTS

This work was supported in part by the ARC Centre of Excellence in Synthetic Biology (CE200100029), the ARC Centre of Excellence in Peptide and Protein Science (CE200100012), the Great Lakes Bioenergy Research Center, U. S. Department of Energy, Office of Science, Office of Biological and Environmental Research under Award Number DE-SC0018409 (S.R and A.T.M) and the NIH Director's New Innovator Award DP2GM132682 (S.R). The content is solely the responsibility of the authors and does not necessarily represent the official views of the NIH, Department of Defense, Department of Energy, or other federal agencies.

AUTHOR CONTRIBUTIONS

A.T.M., M.A.S., C.J.J, and S.R. conceptualized the project. M.A.S. performed the phylogenetic analysis and ancestral protein reconstruction. A.T.M. created designs, performed sorting and NGS experiments, and Rosetta stability calculations. M.A.S. performed binding experiments and operator half-site analyses. M.S. simulated the NK model landscapes. A.T.M., M.A.S., C.J.J, and S.R. drafted the manuscript, A.T.M., and M.A.S. created the figures. C.J.J. and S.R. supervised the work. All authors edited and approved the final manuscript.

711 **REFERENCES**

712 1. Smith, J. M. Natural selection and the concept of a protein space. *Nature* **225**, 563–564
713 (1970).
714 2. de Visser, J. A. G. M. & Krug, J. Empirical fitness landscapes and the predictability of
715 evolution. *Nat. Rev. Genet.* **15**, 480–490 (2014).
716 3. Sarkisyan, K. S. *et al.* Local fitness landscape of the green fluorescent protein. *Nature* **533**,
717 397–401 (2016).
718 4. Romero, P. A. & Arnold, F. H. Exploring protein fitness landscapes by directed evolution. *Nat.*
719 *Rev. Mol. Cell Biol.* **10**, 866–876 (2009).
720 5. Poelwijk, F. J., Kiviet, D. J., Weinreich, D. M. & Tans, S. J. Empirical fitness landscapes
721 reveal accessible evolutionary paths. *Nature* **445**, 383–386 (2007).
722 6. Otwinowski, J., McCandlish, D. M. & Plotkin, J. B. Inferring the shape of global epistasis.
723 *Proc. Natl. Acad. Sci. U. S. A.* **115**, E7550–E7558 (2018).
724 7. Fowler, D. M. & Fields, S. Deep mutational scanning: a new style of protein science. *Nat.*
725 *Methods* **11**, 801–807 (2014).
726 8. Zhou, J. *et al.* Higher-order epistasis and phenotypic prediction. *Proc. Natl. Acad. Sci. U. S.*
727 *A.* **119**, e2204233119 (2022).
728 9. Bloom, J. D. & Arnold, F. H. In the light of directed evolution: pathways of adaptive protein
729 evolution. *Proc. Natl. Acad. Sci. U. S. A.* **106 Suppl 1**, 9995–10000 (2009).
730 10. Weinreich, D. M., Delaney, N. F., Depristo, M. A. & Hartl, D. L. Darwinian evolution can follow
731 only very few mutational paths to fitter proteins. *Science* **312**, 111–114 (2006).
732 11. Campbell, E. *et al.* The role of protein dynamics in the evolution of new enzyme function.
733 *Nature Chemical Biology* **12**, 944–950 (2016).
734 12. Jackson, C. J. *et al.* Conformational sampling, catalysis, and evolution of the bacterial
735 phosphotriesterase. *Proc. Natl. Acad. Sci. U. S. A.* **106**, 21631–21636 (2009).

736 13. Kaczmarski, J. A. *et al.* Altered conformational sampling along an evolutionary trajectory
737 changes the catalytic activity of an enzyme. *Nat. Commun.* **11**, 5945 (2020).
738 14. Nahum, J. R. *et al.* A tortoise-hare pattern seen in adapting structured and unstructured
739 populations suggests a rugged fitness landscape in bacteria. *Proc. Natl. Acad. Sci. U. S. A.*
740 **112**, 7530–7535 (2015).
741 15. Hayashi, Y. *et al.* Experimental rugged fitness landscape in protein sequence space. *PLoS*
742 *One* **1**, e96 (2006).
743 16. Wu, N. C., Dai, L., Olson, C. A., Lloyd-Smith, J. O. & Sun, R. Adaptation in protein fitness
744 landscapes is facilitated by indirect paths. *Elife* **5**, (2016).
745 17. Rodrigues, J. V. *et al.* Biophysical principles predict fitness landscapes of drug resistance.
746 *Proc. Natl. Acad. Sci. U. S. A.* **113**, E1470-8 (2016).
747 18. Flynn, J. M. *et al.* Comprehensive fitness landscape of SARS-CoV-2 Mpro reveals insights
748 into viral resistance mechanisms. *Elife* **11**, (2022).
749 19. Louie, R. H. Y., Kaczorowski, K. J., Barton, J. P., Chakraborty, A. K. & McKay, M. R. Fitness
750 landscape of the human immunodeficiency virus envelope protein that is targeted by
751 antibodies. *Proc. Natl. Acad. Sci. U. S. A.* **115**, E564–E573 (2018).
752 20. Romero, P. A., Krause, A. & Arnold, F. H. Navigating the protein fitness landscape with
753 Gaussian processes. *Proc. Natl. Acad. Sci. U. S. A.* **110**, E193–E201 (2013).
754 21. Gonzalez Somermeyer, L. *et al.* Heterogeneity of the GFP fitness landscape and data-driven
755 protein design. *Elife* **11**, (2022).
756 22. Spence, M. A., Kaczmarski, J. A., Saunders, J. W. & Jackson, C. J. Ancestral sequence
757 reconstruction for protein engineers. *Curr. Opin. Struct. Biol.* **69**, 131–141 (2021).
758 23. Harms, M. J. & Thornton, J. W. Analyzing protein structure and function using ancestral gene
759 reconstruction. *Curr. Opin. Struct. Biol.* **20**, 360–366 (2010).
760 24. Clifton, B. E. *et al.* Evolution of cyclohexadienyl dehydratase from an ancestral solute-binding
761 protein. *Nat. Chem. Biol.* **14**, 542–547 (2018).

762 25. Nguyen, C. C. & Saier, M. H., Jr. Phylogenetic, structural and functional analyses of the LacI-
763 GalR family of bacterial transcription factors. *FEBS Lett.* **377**, 98–102 (1995).
764 26. Monod, J., Wyman, J. & Changeux, J.-P. On the nature of allosteric transitions: A plausible
765 model. *J. Mol. Biol.* **12**, 88–118 (1965).
766 27. Marklund, E. *et al.* Sequence specificity in DNA binding is mainly governed by association.
767 *Science* **375**, 442–445 (2022).
768 28. Otwinowski, J. & Nemenman, I. Genotype to phenotype mapping and the fitness landscape
769 of the E. coli lac promoter. *PLoS One* **8**, e61570 (2013).
770 29. Zuo, Z., Chang, Y. & Stormo, G. D. A quantitative understanding of lac repressor's binding
771 specificity and flexibility. *Quant. Biol.* **3**, 69–80 (2015).
772 30. Barnes, S. L., Belliveau, N. M., Ireland, W. T., Kinney, J. B. & Phillips, R. Mapping DNA
773 sequence to transcription factor binding energy in vivo. *PLoS Comput. Biol.* **15**, e1006226
774 (2019).
775 31. Garruss Alexander, S., Collins Katherine, M. & Church George, M. Deep representation
776 learning improves prediction of LacI-mediated transcriptional repression. *Proceedings of the*
777 *National Academy of Sciences* **118**, e2022838118 (2021).
778 32. Fukami-Kobayashi, K., Tateno, Y. & Nishikawa, K. Parallel evolution of ligand specificity
779 between LacI/GalR family repressors and periplasmic sugar-binding proteins. *Mol. Biol. Evol.*
780 **20**, 267–277 (2003).
781 33. Shimodaira, H. An approximately unbiased test of phylogenetic tree selection. *Syst. Biol.* **51**,
782 492–508 (2002).
783 34. Meinhardt, S. *et al.* Novel insights from hybrid LacI/GalR proteins: family-wide functional
784 attributes and biologically significant variation in transcription repression. *Nucleic Acids Res.*
785 **40**, 11139–11154 (2012).

786 35. Clifton, B. E. & Jackson, C. J. Ancestral Protein Reconstruction Yields Insights into Adaptive
787 Evolution of Binding Specificity in Solute-Binding Proteins. *Cell Chemical Biology* **23**, 236–
788 245 (2016).
789 36. Swint-Kruse, L. & Matthews, K. S. Allostery in the LacI/GalR family: variations on a theme.
790 *Curr. Opin. Microbiol.* **12**, 129–137 (2009).
791 37. Spronk, C. A. *et al.* The solution structure of Lac repressor headpiece 62 complexed to a
792 symmetrical lac operator. *Structure* **7**, 1483–1492 (1999).
793 38. Lehming, N. *et al.* The interaction of the recognition helix of lac repressor with lac operator.
794 *EMBO J.* **6**, 3145–3153 (1987).
795 39. Daber, R. & Lewis, M. Towards evolving a better repressor. *Protein Engineering, Design and*
796 *Selection* **22**, 673–683 (2009).
797 40. Alley, E. C., Khimulya, G., Biswas, S., AlQuraishi, M. & Church, G. M. Unified rational protein
798 engineering with sequence-based deep representation learning. *Nat. Methods* **16**, 1315–
799 1322 (2019).
800 41. Starr, T. N. & Thornton, J. W. Epistasis in protein evolution. *Protein Sci.* **25**, 1204–1218
801 (2016).
802 42. Milk, L., Daber, R. & Lewis, M. Functional rules for lac repressor–operator associations and
803 implications for protein–DNA interactions. *Protein Science* **19**, 1162–1172 (2010).
804 43. Bridgham, J. T., Ortlund, E. A. & Thornton, J. W. An epistatic ratchet constrains the direction
805 of glucocorticoid receptor evolution. *Nature* **461**, 515–519 (2009).
806 44. Pillai, A. S. *et al.* Origin of complexity in haemoglobin evolution. *Nature* **581**, 480–485 (2020).
807 45. Yang, G. *et al.* Higher-order epistasis shapes the fitness landscape of a xenobiotic-degrading
808 enzyme. *Nat. Chem. Biol.* **15**, 1120–1128 (2019).
809 46. Kullback, S. & Leibler, R. A. On Information and Sufficiency. *ann. math. stat.* **22**, 79–86
810 (1951).

811 47. Sadler, J. R., Sasmor, H. & Betz, J. L. A perfectly symmetric lac operator binds the lac
812 repressor very tightly. *Proc. Natl. Acad. Sci. U. S. A.* **80**, 6785–6789 (1983).
813 48. Liao, Q. *et al.* Long time-scale atomistic simulations of the structure and dynamics of
814 transcription factor-DNA recognition. *J. Phys. Chem. B* **123**, 3576–3590 (2019).
815 49. Glasgow, A., Hobbs, H. T., Perry, Z. R., Marqusee, S. & Kortemme, T. Ligand-induced
816 changes in dynamics mediate long-range allostery in the lac repressor. *bioRxiv* (2021)
817 doi:10.1101/2021.11.30.470682.
818 50. Kalodimos, C. G. *et al.* Plasticity in protein-DNA recognition: lac repressor interacts with its
819 natural operator 01 through alternative conformations of its DNA-binding domain. *EMBO J.*
820 **21**, 2866–2876 (2002).
821 51. Zuo, Z. & Stormo, G. D. High-resolution specificity from DNA sequencing highlights
822 alternative modes of Lac repressor binding. *Genetics* **198**, 1329–1343 (2014).
823 52. Stadler, P. F. Landscapes and their correlation functions. *J. Math. Chem.* **20**, 1–45 (1996).
824 53. Stadler, P. F. Fitness landscapes. in *Biological Evolution and Statistical Physics* 183–204
825 (Springer Berlin Heidelberg, 2007).
826 54. Chicano, F., Whitley, L. D. & Alba, E. A methodology to find the elementary landscape
827 decomposition of combinatorial optimization problems. *Evol. Comput.* **19**, 597–637 (2011).
828 55. Hadzipasic, A. *et al.* Ancient origins of allosteric activation in a Ser-Thr kinase. *Science* **367**,
829 912–917 (2020).
830 56. Kaltenbach, M. *et al.* Evolution of chalcone isomerase from a noncatalytic ancestor. *Nat.*
831 *Chem. Biol.* **14**, 548–555 (2018).
832 57. Bar-Rogovsky, H., Hugenmatter, A. & Tawfik, D. S. The evolutionary origins of detoxifying
833 enzymes. *J. Biol. Chem.* **288**, 23914–23927 (2013).
834 58. Castro-Fernandez, V. *et al.* Reconstructed ancestral enzymes reveal that negative selection
835 drove the evolution of substrate specificity in ADP-dependent kinases. *J. Biol. Chem.* **292**,
836 15598–15610 (2017).

837 59. Anderson, D. W., McKeown, A. N. & Thornton, J. W. Intermolecular epistasis shaped the
838 function and evolution of an ancient transcription factor and its DNA binding sites. *Elife* **4**,
839 e07864 (2015).
840 60. Markin, C. J. *et al.* Revealing enzyme functional architecture via high-throughput microfluidic
841 enzyme kinetics. *Science* **373**, eabf8761 (2021).
842 61. Ben-David, M. *et al.* Enzyme evolution: An epistatic ratchet versus a smooth reversible
843 transition. *Mol. Biol. Evol.* **37**, 1133–1147 (2020).
844 62. Capra, E. J., Perchuk, B. S., Skerker, J. M. & Laub, M. T. Adaptive mutations that prevent
845 crosstalk enable the expansion of paralogous signaling protein families. *Cell* **150**, 222–232
846 (2012).
847 63. Zarrinpar, A., Park, S.-H. & Lim, W. A. Optimization of specificity in a cellular protein
848 interaction network by negative selection. *Nature* **426**, 676–680 (2003).
849 64. Liu, Q. *et al.* Ancient mechanisms for the evolution of the bicoid homeodomain's function in
850 fly development. *Elife* **7**, (2018).
851 65. Starr, T. N., Picton, L. K. & Thornton, J. W. Alternative evolutionary histories in the sequence
852 space of an ancient protein. *Nature* **549**, 409–413 (2017).
853 66. McKeown, A. N. *et al.* Evolution of DNA specificity in a transcription factor family produced a
854 new gene regulatory module. *Cell* **159**, 58–68 (2014).
855 67. Srivastava, M. & Payne, J. L. On the incongruence of genotype-phenotype and fitness
856 landscapes. *PLoS Comput. Biol.* **18**, e1010524 (2022).
857 68. Park, Y., Metzger Brian, P. H. & Thornton Joseph, W. Epistatic drift causes gradual decay of
858 predictability in protein evolution. *Science* **376**, 823–830 (2022).
859 69. Yona, A. H., Alm, E. J. & Gore, J. Random sequences rapidly evolve into de novo promoters.
860 *Nat. Commun.* **9**, (2018).
861 70. Fu, L., Niu, B., Zhu, Z., Wu, S. & Li, W. CD-HIT: accelerated for clustering the next-generation
862 sequencing data. *Bioinformatics* **28**, 3150–3152 (2012).

863 71. Notredame, C., Higgins, D. G. & Heringa, J. T-Coffee: A novel method for fast and accurate
864 multiple sequence alignment. *J. Mol. Biol.* **302**, 205–217 (2000).
865 72. Nguyen, L.-T., Schmidt, H. A., von Haeseler, A. & Minh, B. Q. IQ-TREE: a fast and effective
866 stochastic algorithm for estimating maximum-likelihood phylogenies. *Mol. Biol. Evol.* **32**, 268–
867 274 (2015).
868 73. Le, S. Q. & Gascuel, O. An improved general amino acid replacement matrix. *Mol. Biol. Evol.*
869 **25**, 1307–1320 (2008).
870 74. Kalyaanamoorthy, S., Minh, B. Q., Wong, T. K. F., von Haeseler, A. & Jermiin, L. S.
871 ModelFinder: fast model selection for accurate phylogenetic estimates. *Nat. Methods* **14**,
872 587–589 (2017).
873 75. Hoang, D. T., Chernomor, O., von Haeseler, A., Minh, B. Q. & Vinh, L. S. UFBoot2: Improving
874 the Ultrafast Bootstrap Approximation. *Molecular Biology and Evolution* vol. 35 518–522
875 Preprint at https://doi.org/10.1093/molbev/msx281 (2018).
876 76. Yang, Z. PAML 4: Phylogenetic Analysis by Maximum Likelihood. *Molecular Biology and*
877 *Evolution* vol. 24 1586–1591 Preprint at https://doi.org/10.1093/molbev/msm088 (2007).
878 77. Lutz, R. & Bujard, H. Independent and tight regulation of transcriptional units in Escherichia
879 coli via the LacR/O, the TetR/O and AraC/I1-I2 regulatory elements. *Nucleic Acids Res.* **25**,
880 1203–1210 (1997).
881 78. Datsenko, K. A. & Wanner, B. L. One-step inactivation of chromosomal genes in Escherichia
882 coli K-12 using PCR products. *Proc. Natl. Acad. Sci. U. S. A.* **97**, 6640–6645 (2000).
883 79. Zhang, J., Kobert, K., Flouri, T. & Stamatakis, A. PEAR: a fast and accurate Illumina Paired-
884 End reAd mergeR. *Bioinformatics* **30**, 614–620 (2014).
885 80. Bell, C. E. & Lewis, M. A closer view of the conformation of the Lac repressor bound to
886 operator. *Nat. Struct. Biol.* **7**, 209–214 (2000).
887 81. Delgado, J., Radusky, L. G., Cianferoni, D. & Serrano, L. FoldX 5.0: working with RNA, small
888 molecules and a new graphical interface. *Bioinformatics* **35**, 4168–4169 (2019).

82. Lu, X.-J. & Olson, W. K. 3DNA: a versatile, integrated software system for the analysis, rebuilding and visualization of three-dimensional nucleic-acid structures. *Nat. Protoc.* **3**, 1213–1227 (2008).

83. Maier, J. A. *et al.* Ff14SB: Improving the accuracy of protein side chain and backbone parameters from ff99SB. *J. Chem. Theory Comput.* **11**, 3696–3713 (2015).

84. Ivani, I. *et al.* Parmbsc1: a refined force field for DNA simulations. *Nat. Methods* **13**, 55–58 (2016).

85. Hess, B., Bekker, H., Berendsen, H. J. C. & Fraaije, J. G. E. M. LINCS: A linear constraint solver for molecular simulations. *J. Comput. Chem.* **18**, 1463–1472 (1997).

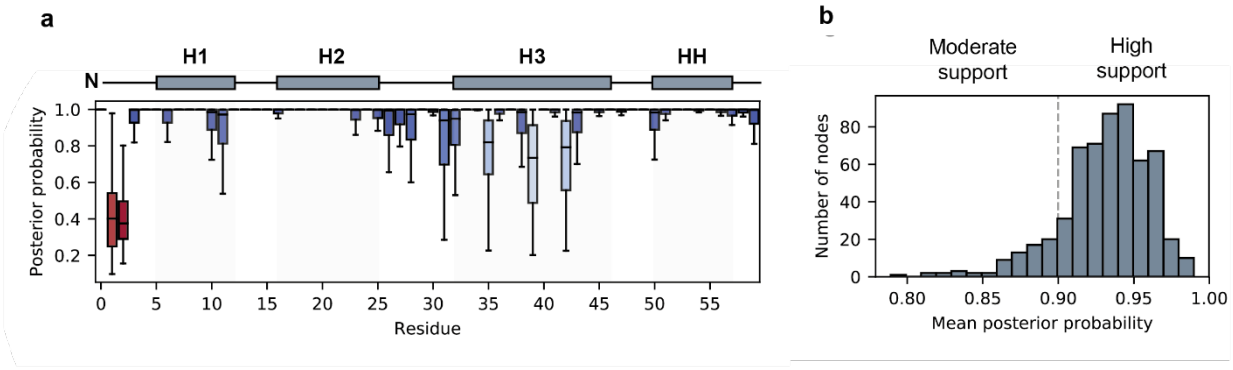

Supplementary Fig. 1. Ancestral sequence reconstruction of prokaryotic transcriptional regulators. (**a**), Site-wise posterior probability distribution averaged over all reconstructed ancestral sequences. (**b**), Distribution of posterior probabilities averaged over the DBD sequence. Most ancestral sequences are reconstructed with high posterior probability (>0.9 mean posterior probability) and very few are reconstructed with less than moderate (<0.8 mean posterior probability). Helix 2 and the hinge-helix, which are most important for DNA-recognition, are reconstructed unambiguously.

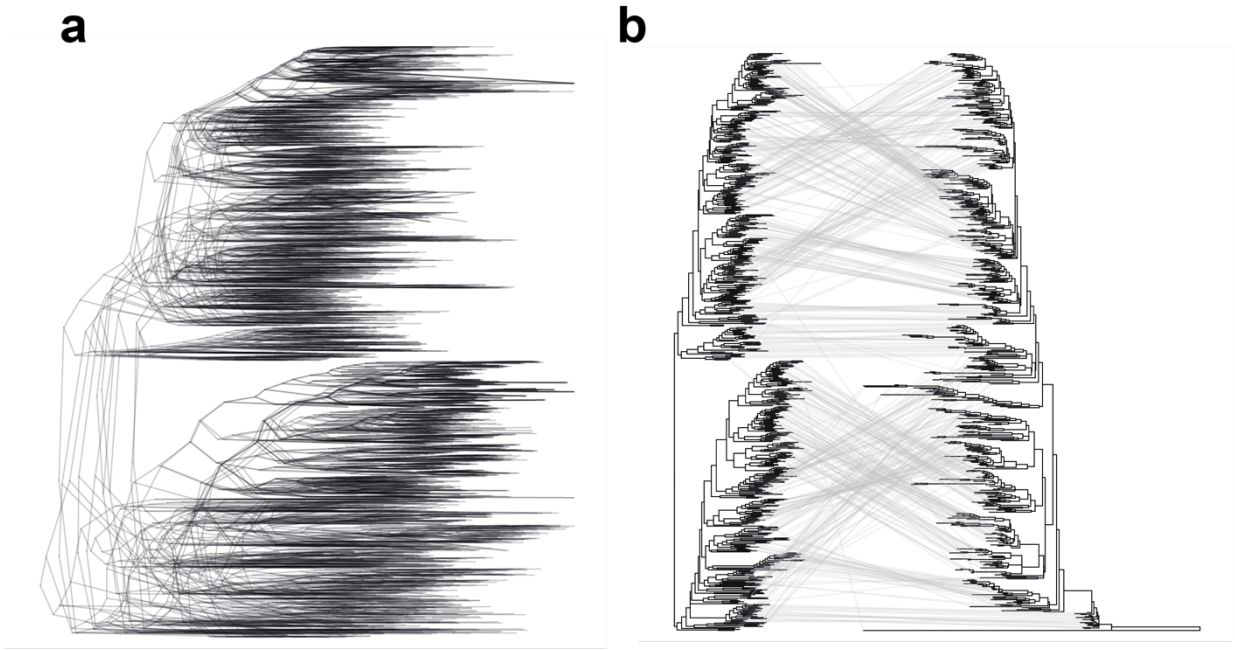

Supplementary Fig. 2. Tree topology testing. (**a**), All 10 reconstructed topologies that passed the AU test conducted to 10000 replicates. Each independent tree search converges on a similar topology. (**b**), Comparison the full DBD and LBD topology presented in main text Fig. 1 (left) and a tree-search performed under the same criteria using only the DBD. Most of the phylogenetic signal in the inference comes from the large LBD sequence, as the DBD-only topology is incongruent with the full-length topology.

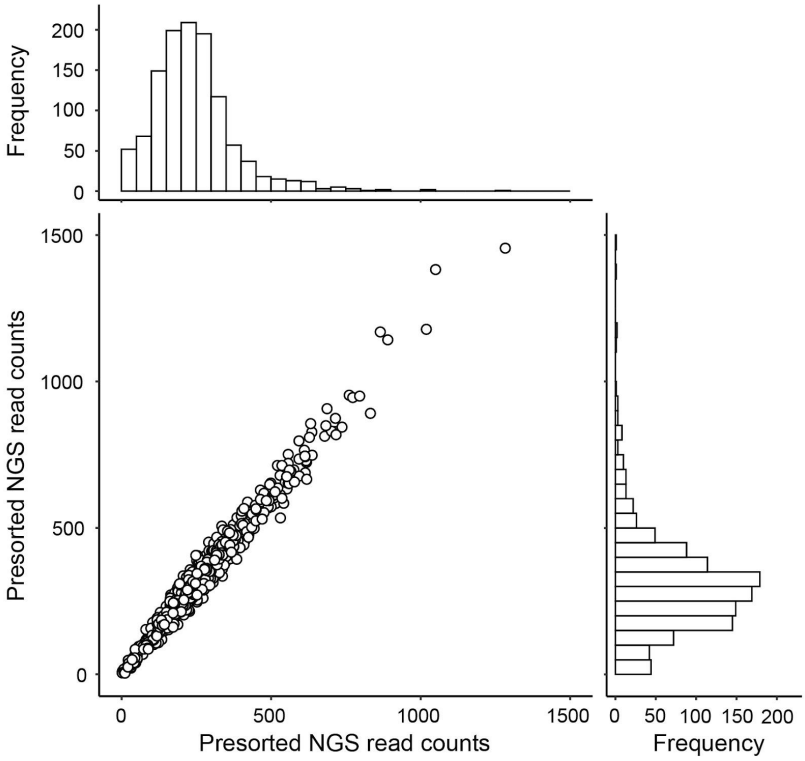

Supplementary Fig. 3. Presorted library distribution of extant and ancestral DBD variants. Raw read counts of all 1158 DBD variants from replicate next-generation sequencing runs (*n*=2). All variants were present in the pooled library (median=250±40 reads) prior to selection of functional repressors. Histograms of presorted read counts show that DBD variants were approximately normally distributed with a moderate right-shift (skewness=1.6±0.1).

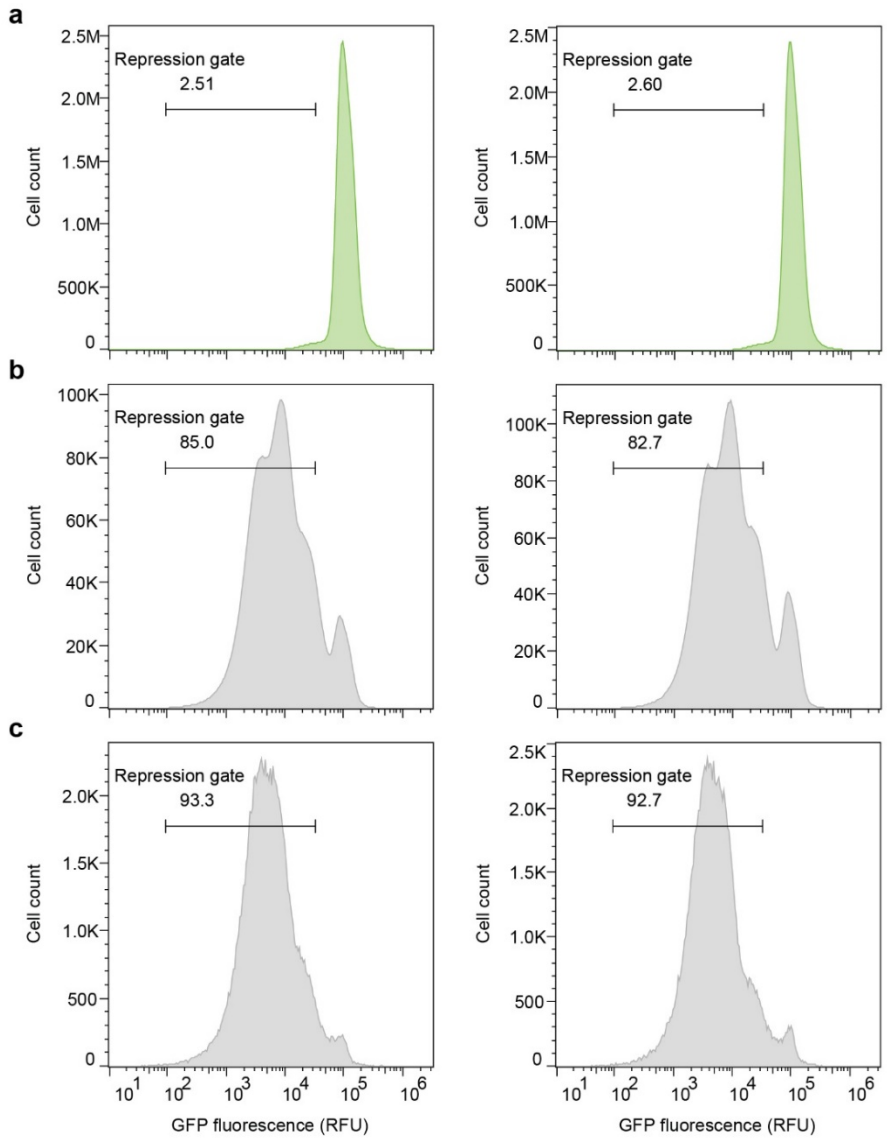

926

927 **Supplementary Fig. 4. Isolation of repression competent extant and ancestral DBDs using**
928 **FACS.** (**a**), Distribution of GFP fluorescence of the pre-selected phylogenetic DBD library using
929 flow cytometry. The small fraction (2.5-2.6%) of low-fluorescence cells shows that relatively few
930 extant and ancestral DBDs library members repress LacO. (**b-c**), Distribution of GFP fluorescence
931 after one (**b**) or two (**c**) rounds of FACS-based selection to isolate the low fluorescence
932 subpopulation. The indicated repression gate was used to enrich for repression competent
933 variants. RFU, relative fluorescence units.

934

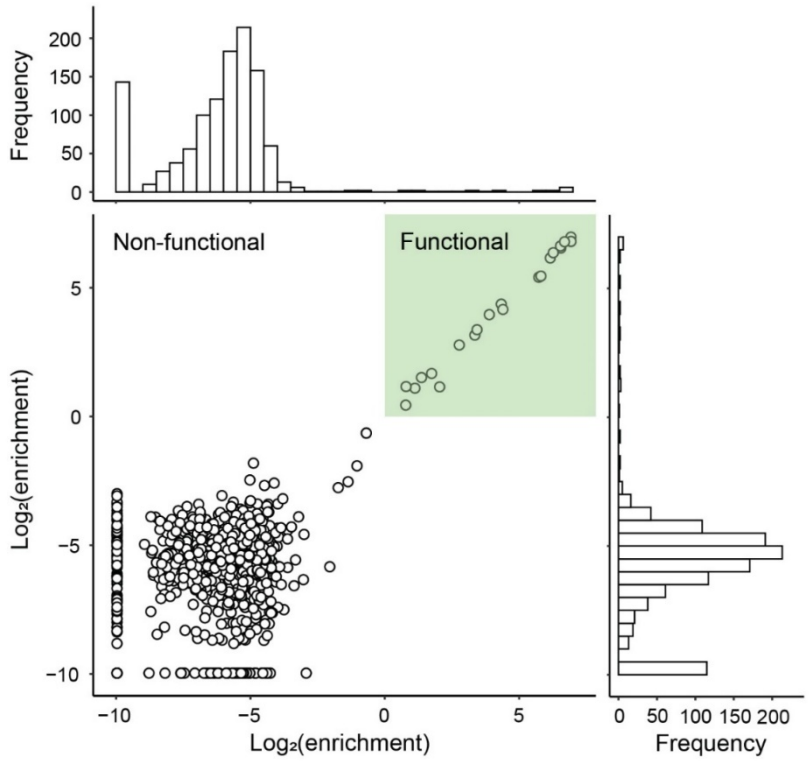

935
936
937 **Supplementary Fig. 5. Post-selection enrichment values of extant and ancestral DBD**
938 **variants.** Log transformed enrichment ratios of all 1158 DBD variants as determined by
939 comparing replicate NGS distributions (*n*=2) of the presorted and sorted populations. Higher
940 enrichment values indicate tighter repression of GFP and increased affinity to LacO. Histograms
941 indicate that few (22 of 1158) DBD variants were enriched and functionally repress LacO (green
942 box).
943

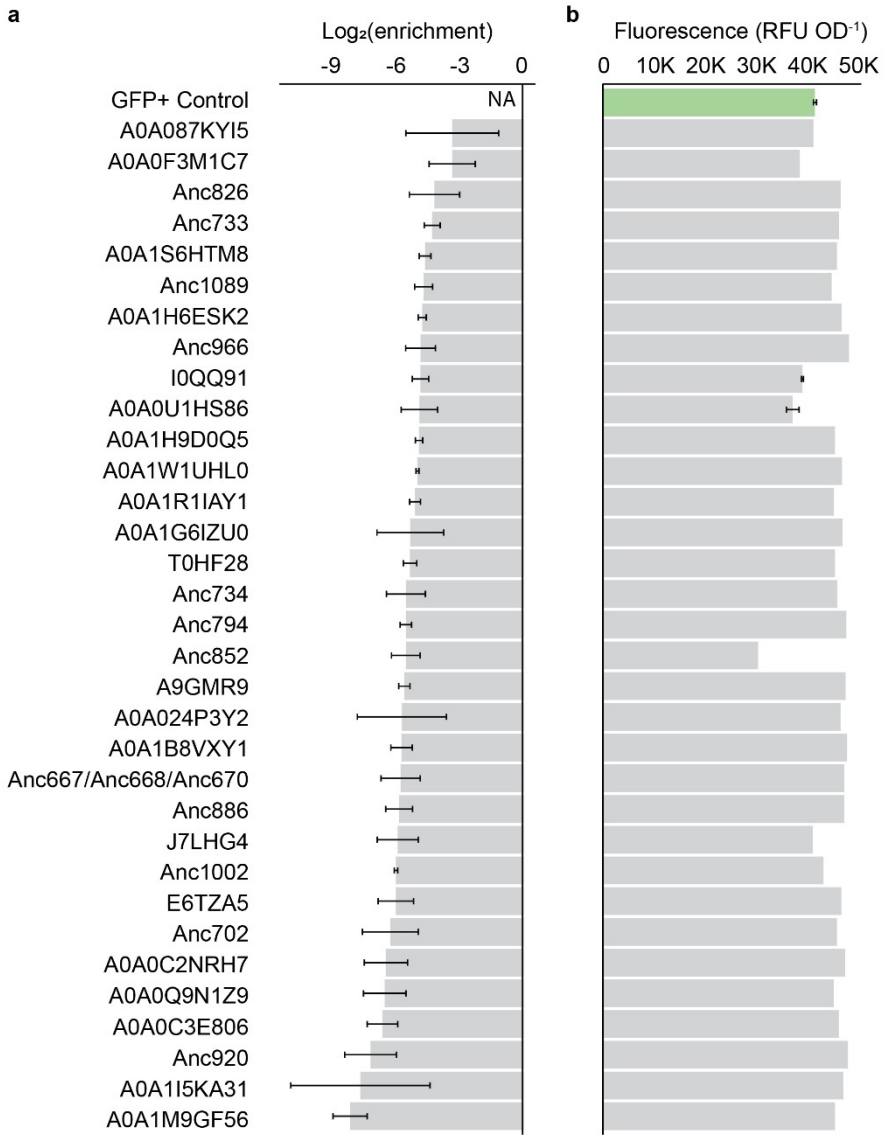

Supplementary Fig. 6. Clonal validation of high-throughput screen. (**a**) Enrichment values of a random subset of depleted ancestral and extant DBD variants derived from the pooled selection and next-generation sequencing experiments. Error bars represent the standard deviation of replicate experiments (*n*=2). (**b**) Clonally assayed mean fluorescence values normalized to OD_{600}. Clones were randomly sampled from the pre-selected population and assayed for GFP repression. All depleted clones exhibit high GFP fluorescence (inability to repress LacO) comparable to our GFP+ reporter cells (green). RFU, relative fluorescence units. OD, optical density.

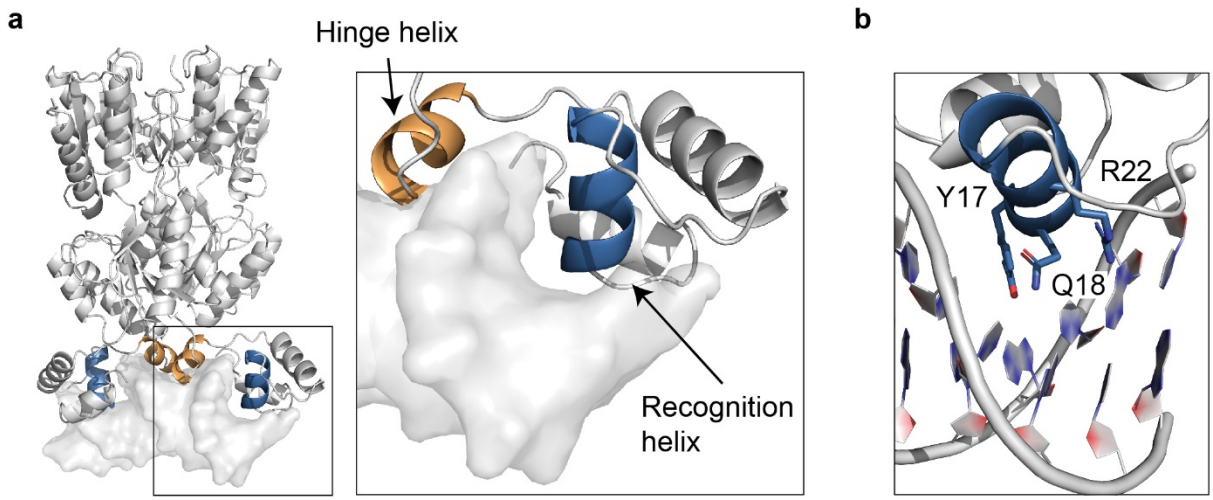

Supplementary Fig. 7. Structural regions of the DBD essential for function. (**a**) Structure (PDB ID: 1EFA) of dimeric extant *E. coli* lac repressor (cartoon) bound to LacO (surface representation). Sequences of functional ancestral and extant DBDs are highly conserved in both the hinge (orange) and recognition helices (blue) (**Fig. 2f**). The hinge helix interacts with the minor groove of LacO, facilitates homodimerization and is involved in allosteric signaling between the LBD and DBD. Functional repressors Anc835, Anc850 and Anc851 are heavily mutated in the hinge helix, but do not relieve GFP repression (**Supplementary Fig. 8**) in the presence of inducer (1mM IPTG), suggesting these mutations may disrupt the allosteric signal transduction pathway. (**b**) Residues of the recognition helix (Y17, Q18, and R22) that facilitate LacO recognition. Y17H and Q18M are the only substitutions tolerated at these critical positions among the functional ancestral and extant DBDs.

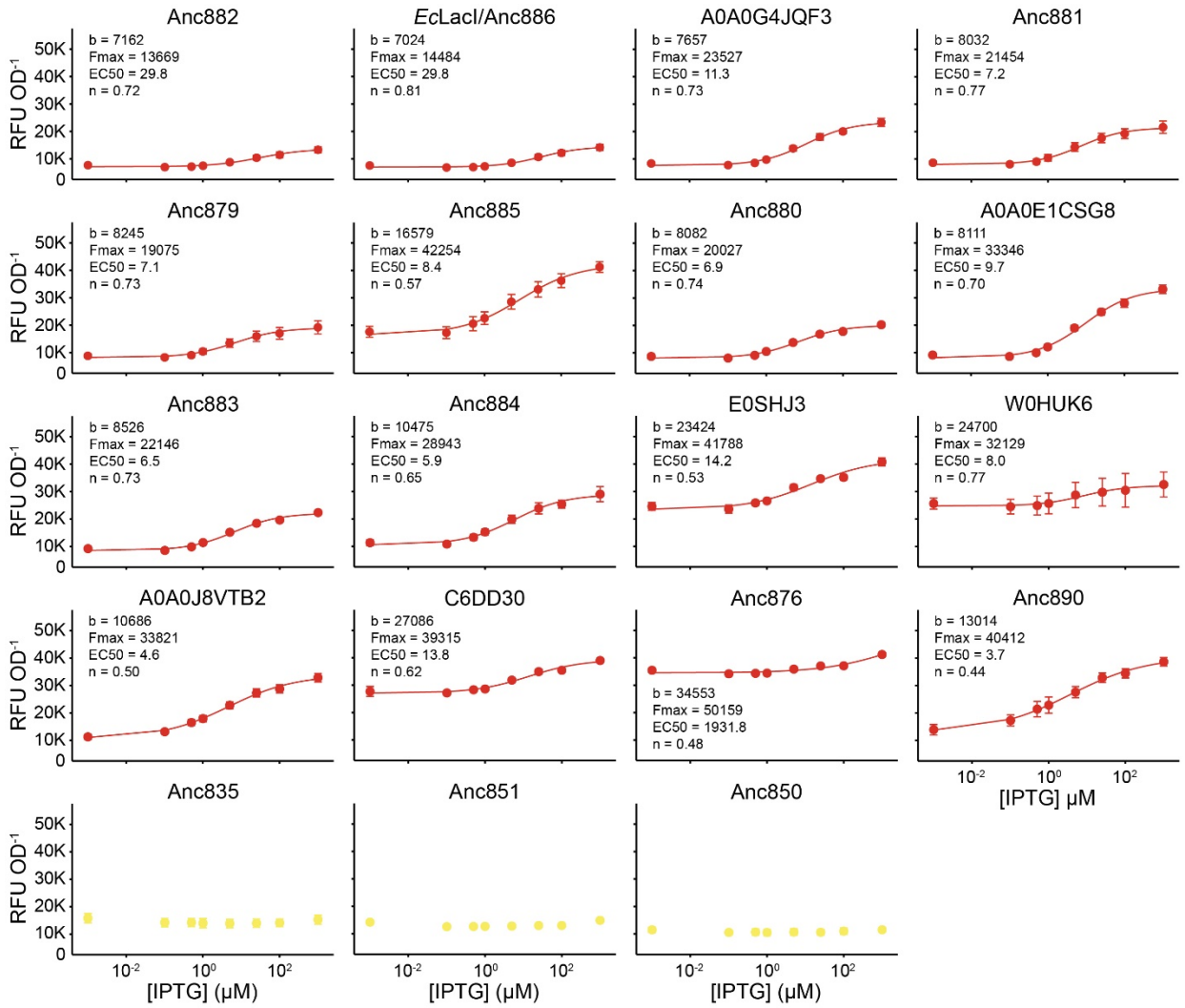

Supplementary Fig. 8. Induction assay of repression competent extant and ancestral DBD variants. The gratuitous inducer IPTG binds to the LBD of *E. coli* LacI to allosterically relieve LacO repression. Dose response curves were fit to the Langmuir-Hill Equation for inducible variants (red). IPTG did not relieve LacO repression for Anc835, Anc851, and Anc850 (yellow). Basal fluorescence, b, is a measure of LacO affinity in the absence of inducer. Fmax is the maximum fluorescence signal achieved at 1mM IPTG. EC50 is the half maximal effective concentration, and n is the Hill coefficient, which is a measure of cooperativity. Error bars represent the standard deviation of replicate experiments ($n \geq 2$).

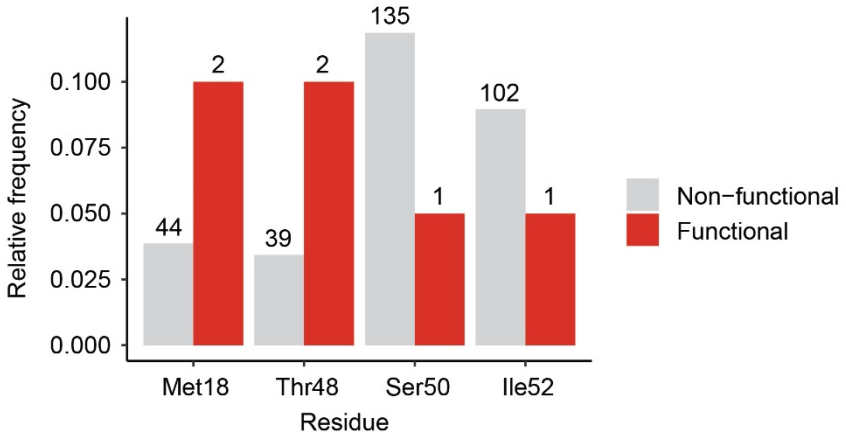

977
978 **Supplementary Fig. 9. Gln18Met substitution provides additional plasticity for LacO**
979 **repression.** Relative amino acid frequencies of Met18, Thr48, Ser50, and Ile52 for non-functional
980 (gray) and functional (red) phylogenetic DBDs. The Gln18Met substitution in *E. coli* LacI has been
981 previously shown to increase affinity to LacO by 2.5-fold.[39] Both functional repressors Anc849
982 and Anc850 have the Gln18Met substitution, and this increased LacO affinity may contribute to
983 the loss of IPTG inducibility (**Supplementary Fig. 8**) and enable less favorable substitutions
984 (Ser50 and Ile52 are more prominent among non-functional DBDs) to be tolerated in Anc851.
985
986

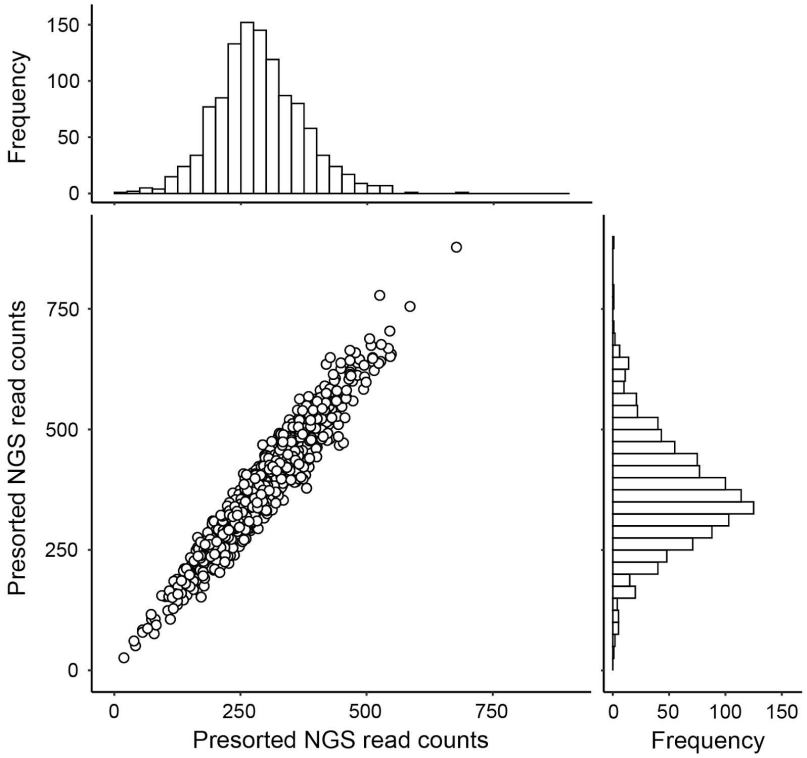

Supplementary Fig. 10 Presorted library distribution of *E. coli* LacI DBD deep mutational scanning variants. Raw read counts of all 1121 DBD single mutant variants from replicate next-generation sequencing runs (*n*=2). All DMS variants were present in the pooled library (median=320±50 reads) prior to selection of functional repressors. Histograms of presorted read counts show that DBD variants were approximately normally distributed with minimal skew (skewness=0.38±0.04).

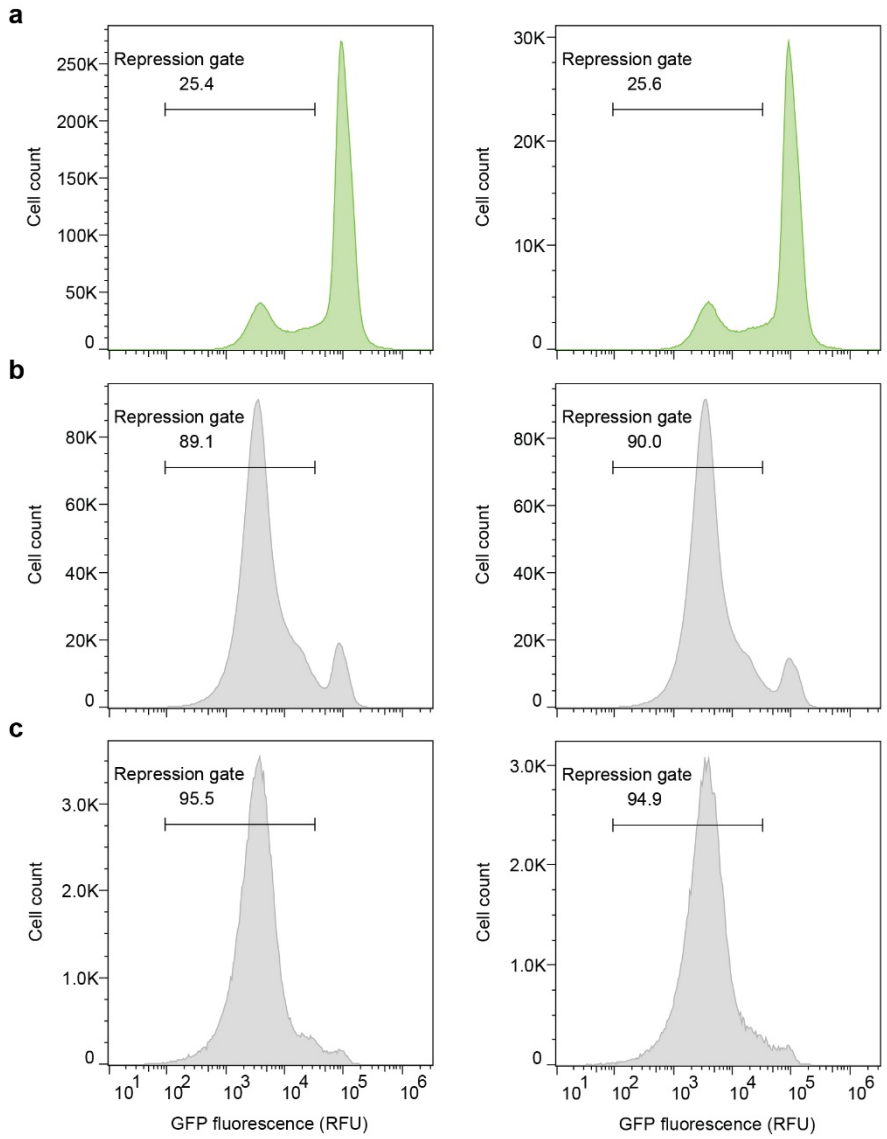

Supplementary Fig. 11. Isolation of repression competent *E. coli* LacI DBD deep mutational scanning variants using FACS. (**a**), Distribution of GFP fluorescence of the pre-selected library using flow cytometry. A larger fraction of low-fluorescence cells (25.4-25.6%) was observed for the DMS library than the phylogenetic library, which indicates that many more DMS variants repress LacO. (**b-c**), Distribution of GFP fluorescence after one (**b**) or two (**c**) rounds of FACS-based selection to isolate the low fluorescence subpopulation. The indicated repression gate was used to enrich for repression competent variants. RFU, relative fluorescence units.

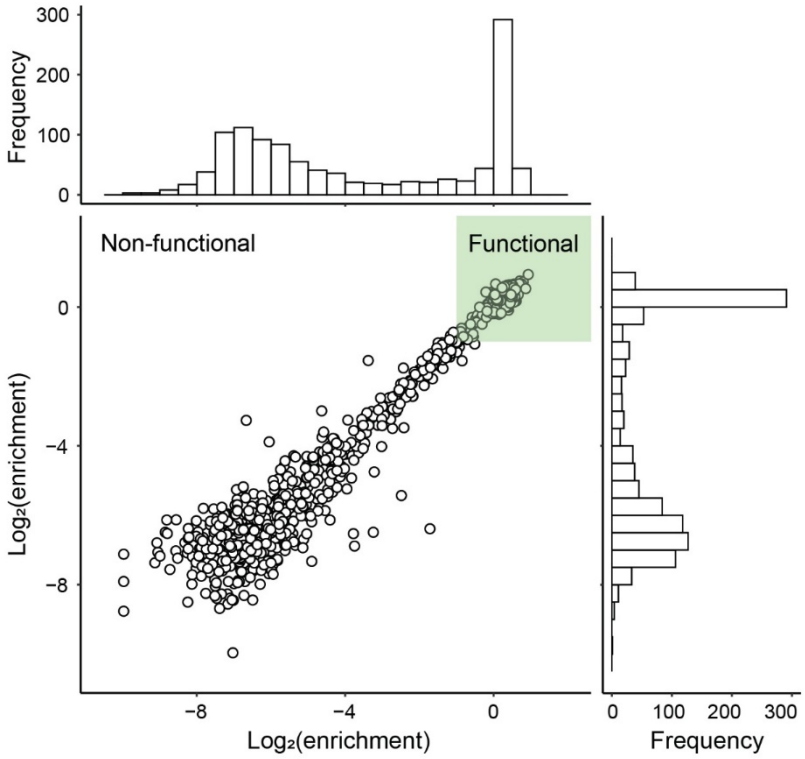

Supplementary Fig. 12. Post-selection enrichment values of *E. coli* LacI DBD deep mutational scanning variants. Log transformed enrichment ratios of all 1158 DBD variants as determined by comparing replicate NGS distributions (*n*=2) of the presorted and sorted populations. Higher enrichment values indicate tighter repression of GFP and increased affinity to LacO. Histograms indicate that 400 (35%) DBD variants were enriched and functionally repress LacO (green box).

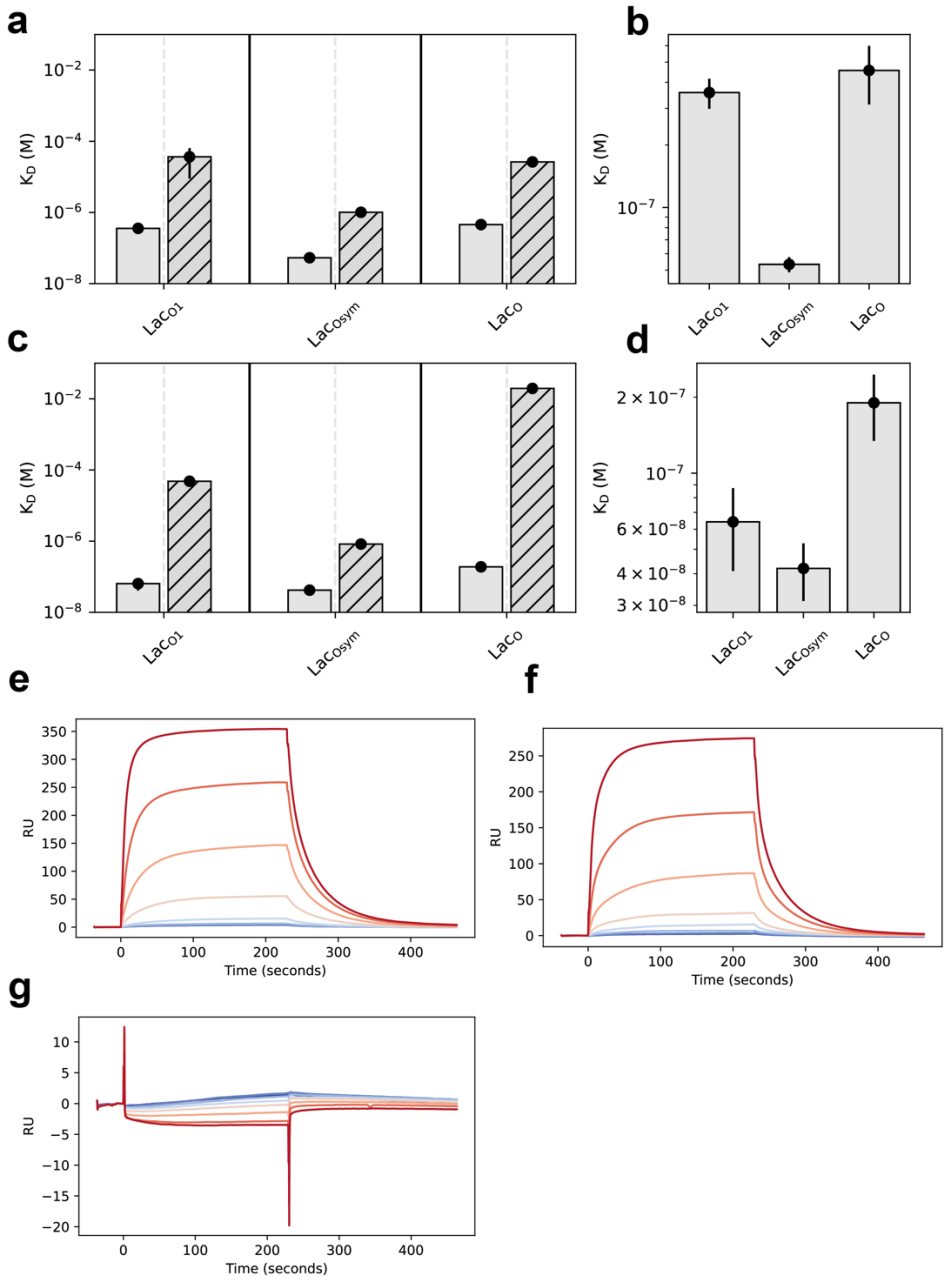

Supplementary Fig. 13 Surface plasmon resonance kinetics and sensograms. (a) K_d constants of Anc880 for $LacO_1$, $LacO_{sym}$ and LacO when repressed (solid) and induced with 70 μM IPTG (hashed). (b) Zoomed in view of repressed K_d constants for Anc880 binding. (c) K_d constants of Anc881 for $LacO_1$, $LacO_{sym}$ and LacO when repressed (solid) and induced with 70 μM IPTG (hashed). (d)) Zoomed in view of repressed K_d constants for Anc881 binding. (e) Sensogram for Anc880 LacO binding at protein concentrations of 250 nM – 3.91 nM in a log2 dilution series. (f) Sensogram for Anc881 LacO binding at protein concentrations of 250 nM –

1021 3.91 nM in a log2 dilution series. (g) Sensogram for Anc882 binding random DNA at protein
1022 concentrations of 250 nM – 3.91 nM in a log2 dilution series**.** There is no detectable binding for
1023 random DNA.

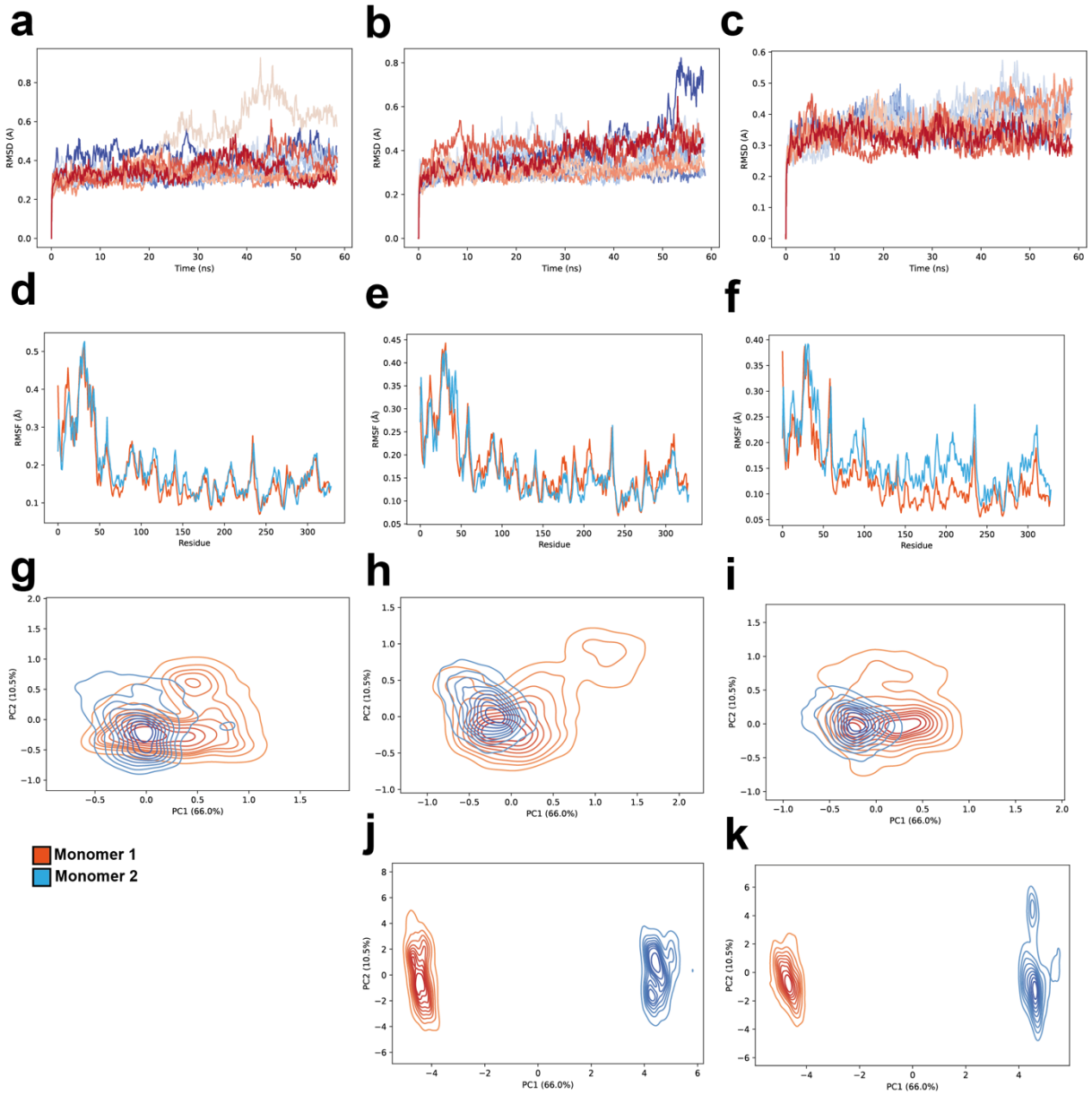

Supplementary Fig. 14. Molecular dynamics simulations of Anc880, Anc882 and EcLacI. (a – c). RMSD evolution of Anc882, Anc880 and EcLacI, respectively. The 10 independent replicates are distinguished by colour. (d-f) RMSF split by monomer for Anc882, Anc880 and EcLacI, respectively. (g-i) PCA of backbone alpha carbons within only the DBD for Anc882, Anc880 and EcLacI, respectively. (j-k) PCA of backbone alpha carbons over the full regulator structure for Anc880 and EcLacI.

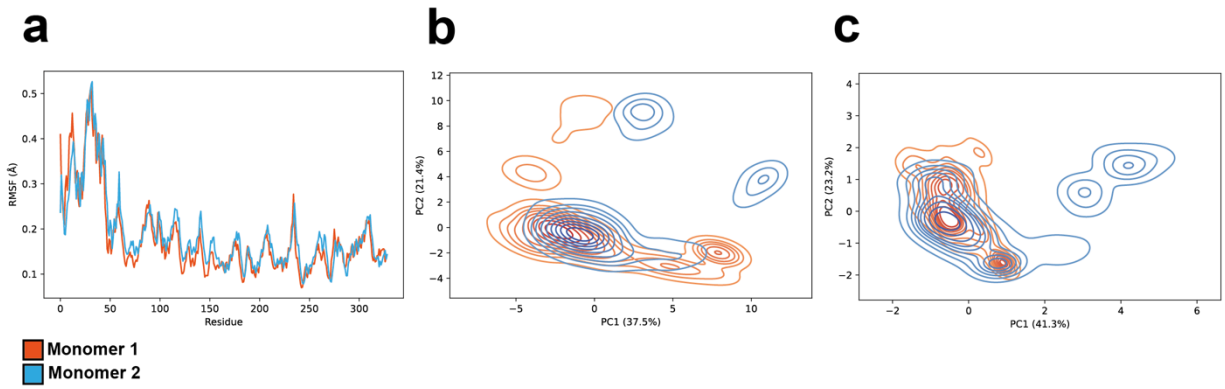

Supplementary Fig. 15. Molecular dynamics simulations of apo-Anc882. (a) RMSF of apo-Anc882 trajectories split by monomer. (b) PCA of backbone alpha carbons over the full apo-Anc882 structure. (c) PCA of backbone alpha carbons over the apo-Anc882 DBD. Motions between monomers in the apo-Anc882 trajectory are highly similar.